2013

Metallic and Ceramic Thin Film Thermocouples

Ian M. Tougas
University of Rhode Island, itougas007@gmail.com

METALLIC AND CERAMIC THIN FILM THERMOCOUPLES

BY

IAN M. TOUGAS

A THESIS SUBMITTED IN PARTIAL FULFILLMENT OF THE

REQUIREMENTS FOR THE DEGREE OF

MASTER OF SCIENCE

IN

CHEMICAL ENGINEERING

UNIVERSITY OF RHODE ISLAND

2013

MASTER OF SCIENCE IN CHEMICAL ENGINEERING THESIS

OF

IAN M. TOUGAS

APPROVED:

Thesis Committee:

Major Professor Otto Gregory

Hamouda Ghonem

Everett Crisman

David Heskett

Nasser H. Zawia
DEAN OF THE GRADUATE SCHOOL

UNIVERSITY OF RHODE ISLAND
2013

ABSTRACT

Operating temperatures in the hot sections of modern gas turbine engines reach as high as 1500°C, making *in situ* monitoring of the severe temperature gradients on the surface of components rather difficult. Therefore, there is a need to develop thermocouples which can stably measure temperature in these harsh environments. Refractory metal and ceramic thin film thermocouples are well suited for this task since they have chemical and electrical stability at high temperatures in oxidizing atmospheres, they are compatible with thermal barrier coatings employed on engine components, have higher sensitivity than conventional wire thermocouples, and they are non-invasive to the engine environment. In this masters thesis, thin film combinatorial chemistry for materials discovery and characterization was the primary tool used to optimize thermo-element materials for thin film thermocouples. The resulting sensors based on ceramics, such as indium oxide and indium tin oxide, as well as others based on refractory metals, such as platinum and palladium, exhibited remarkable stability for many cycles at temperatures above 1000°C.

ACKNOWLEDGMENTS

I would like to formally distinguish Dr. Otto J. Gregory for the outstanding guidance and expertise, as an advisor and professor; he has given me at the University of Rhode Island during the four years of my undergraduate and graduate research assistantship. He has inspired me to achieve demanding goals beyond my expectations through various research projects, the completion of many courses in engineering and materials science, and through publishing manuscripts in well known scientific journals. Furthermore, I would like to thank the members of my thesis committee, Dr. Everett E. Crisman, Dr. Hamouda Ghonem, and Dr. David Heskett for their help in the completion of my masters thesis program in chemical engineering.

I could not have completed the work contained in this thesis without the help of my fellow researchers at the URI Center for Sensors and Instrumentation Research: Michael Platek, Mitchell Beck, Yun Chu, Ximing Chen, Emily Moorehead, Robert Balikov, and Matin Amani. Additionally, I would like to thank our partners who provided the research grants I worked under over the past four years: Mesoscribe Technologies, Inc. of Saint James, NY, NASA Glenn Research Center of Cleveland, Ohio, and Rolls-Royce Indianapolis. Finally, I would like to thank Sheryl Girard and Brenda Moyer of the URI department of chemical engineering for their support and help in my academic and research efforts.

PREFACE

The work presented in this thesis is the continuation of the high temperature sensors research pioneered by Dr. Gregory and his research group for the past thirty years at URI. This thesis is presented in manuscript format with an introductory chapter one, three manuscripts as chapters two through four, and a fifth chapter highlighting ideas for the future continuation of this work. Chapters two present a manuscript on the stability of indium tin oxide based thermocouples. Chapter three contains a manuscript on the use of thin film combinatorial chemistry techniques for optimizing the thermoelectric properties of Cu-In-O based thermocouples. The fourth chapter presents an investigation of platinum-palladium thin film thermocouples. Lastly, chapter five elaborates on the future work which can be performed to further develop the work presented in this thesis.

Chapter one gives an introduction to thin film instrumentation of gas turbine engines, an overview of thin film combinatorial chemistry and how it was developed for the work in this thesis, and an elaboration on how the thermocouples in the three manuscripts were tested.

Chapter two presents the first manuscript, “Stability and Microstructure of Indium Tin Oxynitride Thin Film Thermocouples” by Otto J. Gregory, Matin Amani, Ian M. Tougas, and Alvin J. Drehman which discusses improvements to the thermoelectric stability of thin film thermocouples based on indium oxide and indium tin oxide and the resulting microstructures of the films. More specifically, reactive sputtering of indium oxide and indium tin oxide in nitrogen was used to metastably retain nitrogen in the films to form indium oxynitride or indium tin oxynitride. The slower sintering

kinetics of nitrides relative to oxides was utilized to inhibit microstructural changes during thermal cycling, which often leads to sensor instability. This manuscript is currently published in the *Journal of the American Ceramic Society* (Volume 95, Issue 2, pages 705-710 February 2012).

Chapter three contains the second manuscript, "Thermoelectric Properties and Microstructure of Cu-In-O Thin Films" by Otto J. Gregory, Ian M. Tougas, Matin Amani, and Everett E. Crisman. It presents the thermoelectric properties of hundreds of thin films in the CuO-In_2O_3 system using combinatorial sputtering techniques. Optimized p-type and n-type semiconducting materials were rapidly identified, a characteristic that is difficult to achieve using any technique in a single binary oxide system. Furthermore, it demonstrates the merits of using thin film combinatorial chemistry to identify ideal thermoelectric materials, such as a p-type and n-type material, to produce stable, high output thermocouple junctions. This manuscript is currently being reviewed by the *Journal of Electronic Materials* for publication.

Chapter four presents the third manuscript, "Thin film platinum-palladium thermocouples for gas turbine engine applications" by Ian M. Tougas and Otto J. Gregory where the thermoelectric properties and microstructures of platinum-palladium thin film thermocouples are presented. These sputtered thermocouples were found to be more stable than any other metal thin film thermocouple to date, including the type-S thin film thermocouple (platinum-platinum/10% rhodium) that is currently the aerospace industry standard. Furthermore, the stability of these thin film thermocouples was on the same order as conventional wire thermocouples (type-K) operating in the same temperature range (above 1000°C). This manuscript is currently

being reviewed by *Thin Solid Films* for publication. Additionally, a provisional filing for a United States patent based on this technology has been filed.

Chapter five discusses future ideas for the continuation of the work presented in this thesis. Research using both ceramic and metal thin film thermocouples in terms of modern gas turbine engine requirements is elaborated on as well as the current state of the ongoing work involving thermoelectric Cu-In-O thin films.

A provisional United States patent based on the implementation of thin film sensors, such as those studied in this thesis, on the surface of SiC-SiC ceramic matrix composites (CMC) has been filed.

TABLE OF CONTENTS

LIST OF TABLES

TABLE PAGE

LIST OF FIGURES

CHAPTER 1

INTRODUCTION

1.1 Thin Film Instrumentation of Gas Turbine Engines

The next generation of gas turbine engine technology, used for propulsion and energy generation systems, is utilizing increasingly advanced materials which are designed to handle the harsh environments inside these engines. With advances in engine materials comes the need for developing new instrumentation which can handle the harsher environment and monitor the operating conditions inside the engine during testing. Designers must gain an understanding of the operating conditions and perform diagnostics in order to ensure an engine is safe for use in an aircraft or other application. More specifically, technological advancement in gas turbine engine technology brings several improvements such as lighter engine components with superior thermomechanical properties, more advanced thermal barrier coatings (TBC) for components such as the turbine blades, and higher operating temperatures to improve overall combustion efficiency and reduce harmful emissions. Therefore, design and implementation of sensors which will be used to monitor operating conditions and perform diagnostics in these modern engines is becoming an increasingly difficult task.

Many issues arise when attempting to integrate sensors inside modern gas turbines, especially since they operate with severe conditions such as supersonic nozzle velocities, rotational forces exceeding fifty thousand g, and temperatures which

reach as high as 1500°C in the hot section. Conventional wire sensors cannot reliably withstand these conditions due to their geometrical interference with combustion gas flow patterns and vibrational modes of rotating parts. Furthermore, they also require high temperature adhesives to integrate them into engine components. As an alternative, research efforts have focused on thin film sensors to replace conventional wire sensors. Thin films not only avoid many of the issues invoked by wire sensors but also introduce other advantages. They do not interfere with gas flow patterns because their thicknesses, on the order of micrometers, lie below the boundary layer thickness formed on instrumented engine component surfaces, which is below 1 mm, and with masses on the order of micrograms, they do not affect the vibrational modes of rotating parts. In addition, their properties are not affected by the rotational forces inside the engine and they also have much faster signal response times due to low thermal mass relative to wire sensors. Thin films can be directly deposited onto the surface of components without surface preparation and the need for high temperature adhesives. In this way, more accurate surface measurements can be made.

Temperature measurements on the surface of gas turbine engine components during operation is an integral part of the testing effort which goes into each gas turbine engine prior to implementation on an aircraft or in a power generation application. Thin film thermocouples have been developed to provide stable temperature measurements during engine testing and diagnostics. A thermocouple is comprised of a metallurgical junction of two dissimilar materials which produces a net voltage output as a function of the applied temperature difference along the thermoelements. This concept is illustrated in figure 1. Additionally, figure 2 shows a

J85 engine testing setup using thin film thermocouples and figure 3 shows a thin film thermocouple like those developed for the work in this thesis. Thermo-element materials based on refractory noble metals and semiconducting ceramics are promising candidates for instrumentation of modern gas turbine engines. These materials have high melting temperature and chemical and electrical stability at high temperatures in oxidizing atmospheres. Additionally, they have excellent thermal expansion coefficient compatibility with TBCs which are applied to the surface of engine components. The work in this thesis presents further enhancements to the current state of thin film thermocouple technology for gas turbine engines, using both ceramic and metal based thin film thermocouples by improving stability. Additionally, thin film combinatorial chemistry techniques were developed as a materials discovery method for optimizing the thermoelectric properties of thin film thermocouples in a particular material system of interest.

1.2 Thin Film Combinatorial Chemistry

Thin film combinatorial chemistry techniques were developed for the manuscripts in this thesis to screen potential candidate thermo-element materials for use in thin film thermocouples. Specifically, these techniques involved the simultaneous deposition of hundreds of thermocouples, each with a unique composition, in a material system of choice. It was done in such a way that the thermoelectric properties of each could be rapidly screened and optimized compositions for thermo-element materials could be identified quickly. Traditionally, hundreds of sputtering targets with unique compositions would have been required to

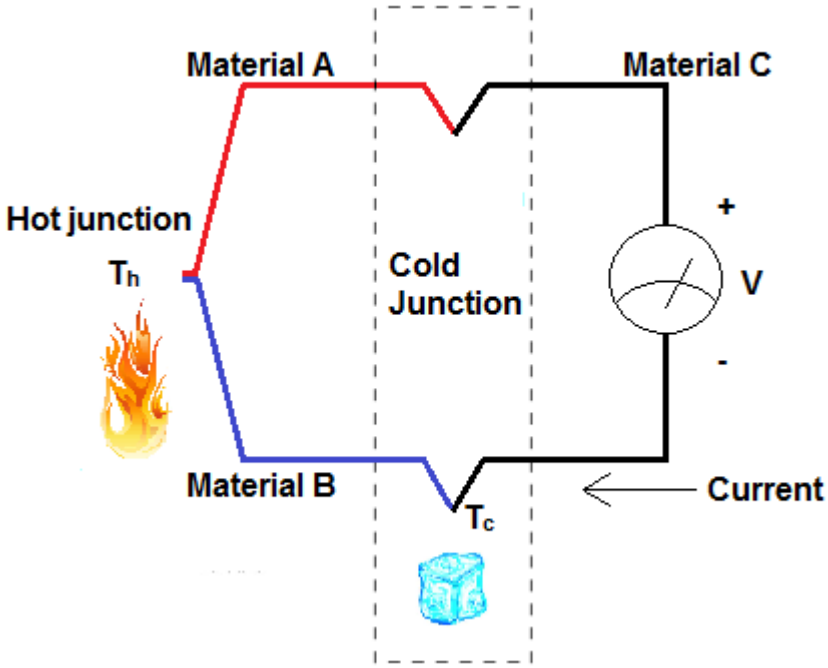

Figure 1. Thermocouple measurement circuit showing the junction of two dissimilar materials subject to a temperature difference along its length. The resulting thermoelectric voltage is measured as a function of the applied temperature difference.

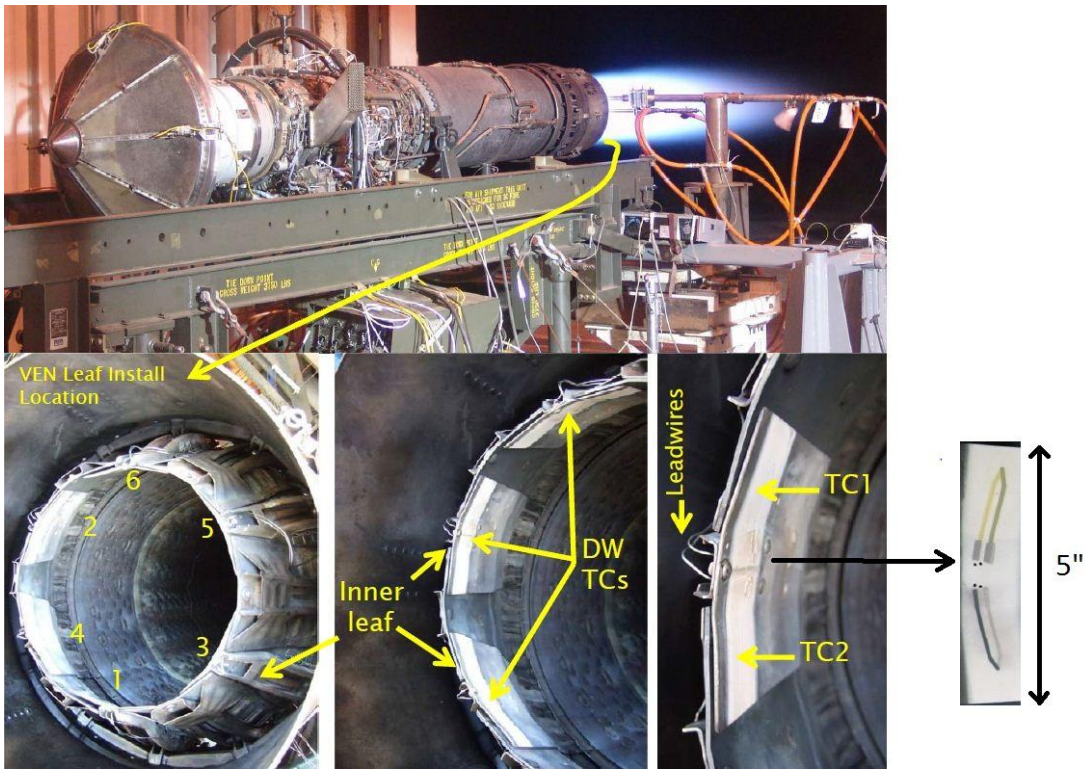

Figure 2. General Electric J85 engine test setup instrumented with thin film thermocouples. Lead wires were embedded in the root of the parts containing thermocouples to retrieve voltage signals during thermal cycling. (Image provided by MesoScribe Technologies, Inc.)

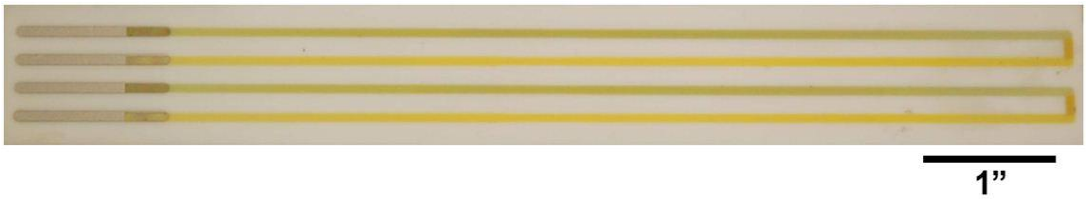

Figure 3. Two thin film thermocouples fabricated by radio frequency sputtering onto a ceramic substrate. Length of beam is 7 inches.

test the individual properties of each thermocouple material, which in this case was completed in a single sputtering run.

In order to accomplish this, a ceramic substrate was covered with a photoresist film and hundreds of windows in the shape of thermoelectric junctions were created using photomasking, exposure, and development. The substrate was then placed between two simultaneously energized sputtering targets separated by 27.3 cm, which represented the end members of a particular material system of interest. Then a single sputtering run resulted in the deposition of hundreds of thermocouples in that material system to form a combinatorial library. Each library element had a slightly different composition relative to its nearest neighbor as a result of the composition gradient formed between the two end members. The spatial dependence of each window in the photoresist film dictated the composition of a particular sputtered thin film, whereby if it was closer to one sputtering target it would be richer in that material and vice versa. A typical combinatorial library fabricated using this method is shown in figure 4 and the sputtering environment developed for this thin film combinatorial chemistry procedure is shown schematically in figure 5. The thermoelectric properties of each thermocouple in the library were then rapidly screened to find the most promising compositions in the material system. This was done by establishing a temperature difference along the length of the thermocouple using a hot probe and measuring the thermoelectric voltage using a data acquisition system instrumented with probes. Compositions of the thermocouples with promising or optimized thermoelectric properties were determined using energy dispersive spectroscopy or Auger electron spectroscopy. Typically, not every library thermo-element composition of interest was

determined; however a statistically sufficient number of thermocouple compositions were measured to model the full range of interest. Custom sputtering targets of the most promising materials could then be made using powder processing techniques. Powders of each end member material were combined in the appropriate ratio, mixed in a ball mill for 24 h, uniaxially pressed, and sintered in a high temperature furnace. The thermocouple geometry shown in figure 4 could be scaled up to something more comparable to the dimensions of a gas turbine blade (figure 3). A flow chart of the combinatorial chemistry procedure developed for the work in this thesis is shown in figure 6. The combinatorial chemistry techniques detailed above were fundamental to the success of optimizing thermocouple materials in the In_2O_3-SnO_2 and CuO-In_2O_3 systems.

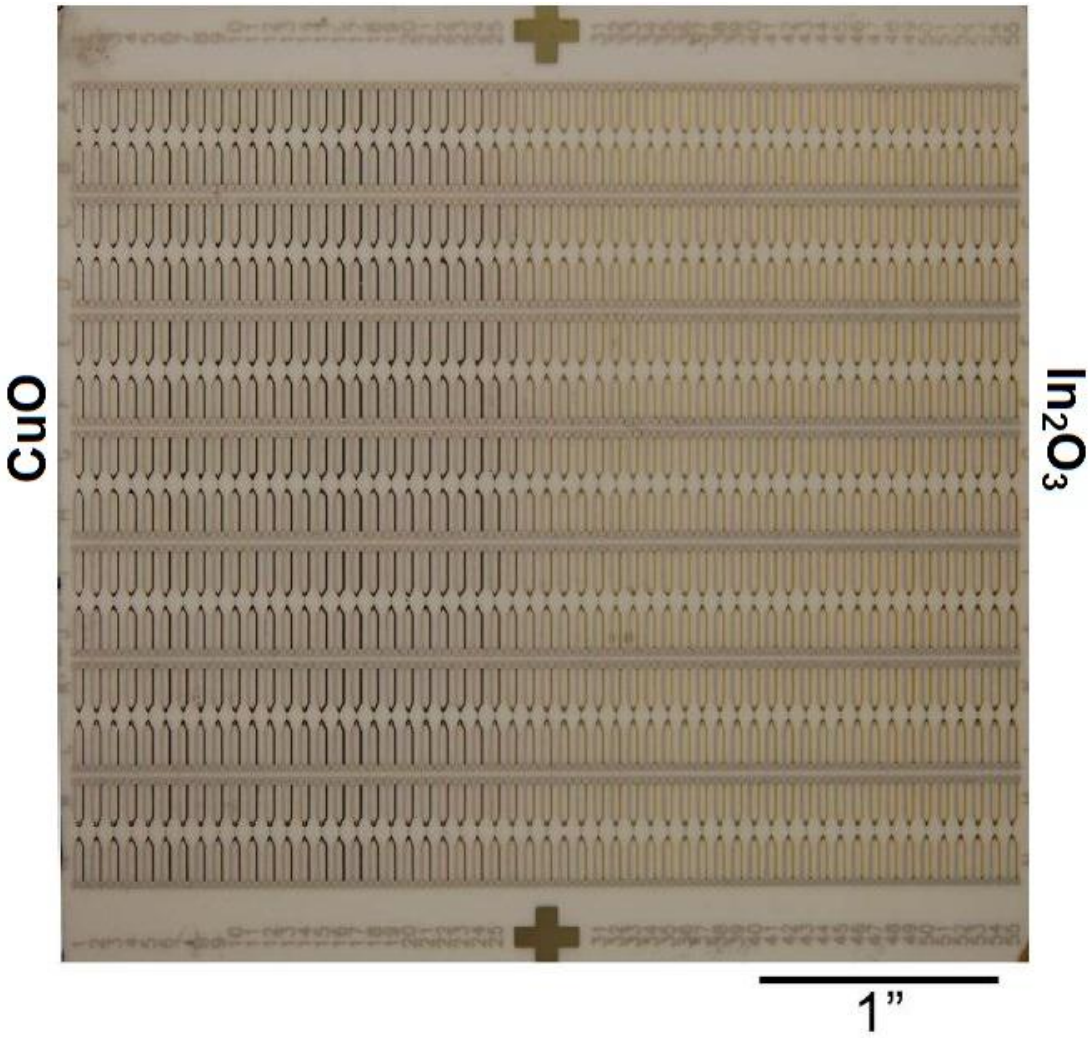

Figure 4. Combinatorial library fabricated by simultaneous sputtering from CuO and In_2O_3 targets. A composition gradient (note the color change of the thermoelements from left to right) was formed between the two targets resulting in the fabrication of several hundred thermocouples with unique compositions in a single sputtering run.

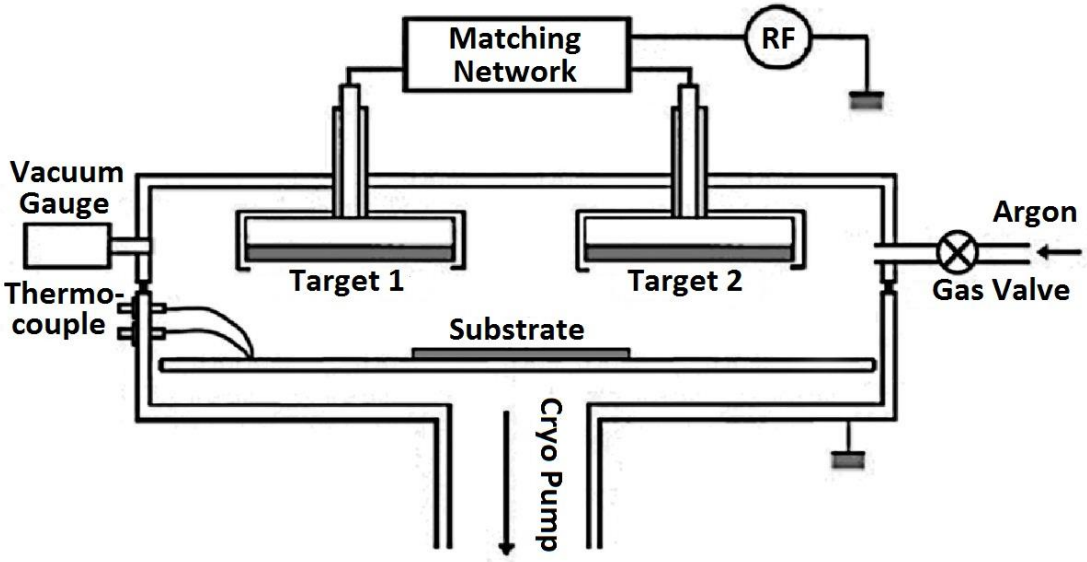

Figure 5. Schematic of the thin film combinatorial sputtering setup. Both targets are simultaneously energized with equal radio frequency power and the patterned substrate is placed equidistant from each target. The pattern contains hundreds of windows in a photoresist film, each with a different position relative to each target. This results in a unique, position dependent composition formed in each window.

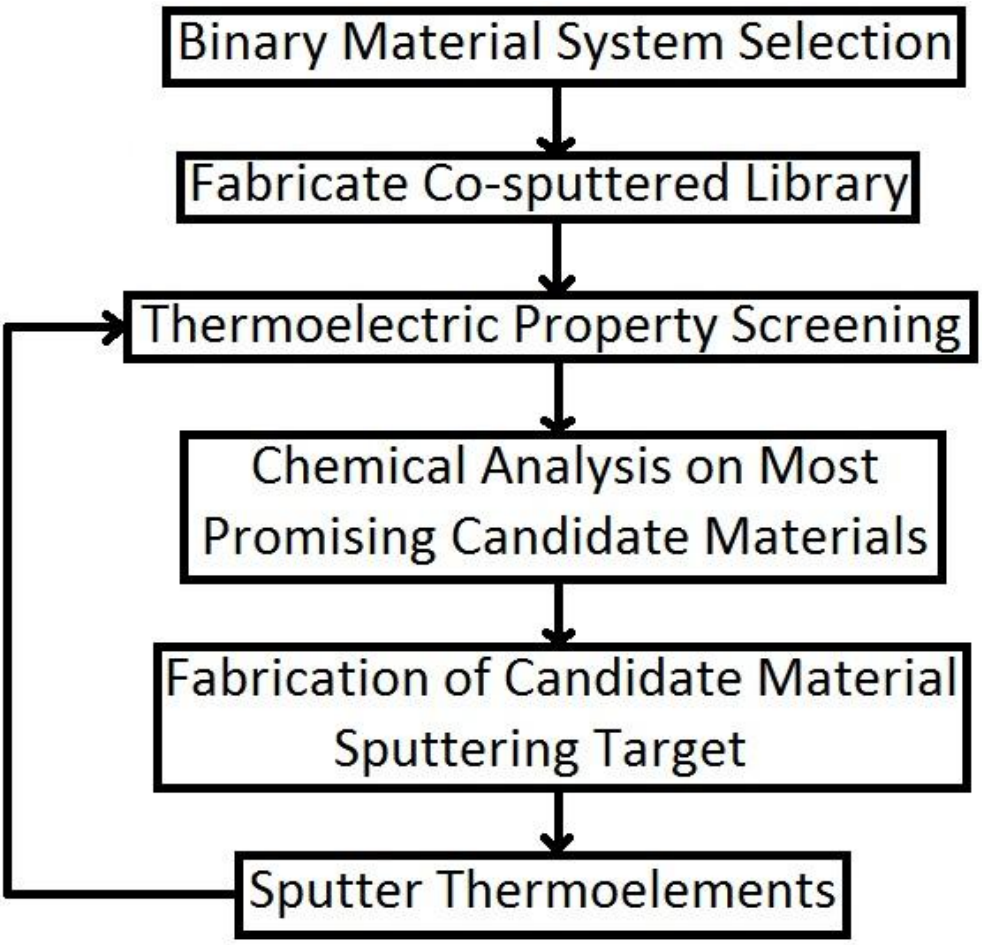

Figure 6. Flow chart of the thin film combinatorial chemistry procedure developed for the work in this thesis.

1.3 Thermocouple testing

The thermocouples used to collect data for the manuscripts in chapters two and four in this thesis were fabricated on ceramic beams using radio frequency sputtering and tested using a custom tube furnace rig. The rig simulates the temperature gradient impose along the length of the components inside the hot section of a gas turbine engine. The rig use for the work in this thesis could achieve peak temperatures of 1400°C and differences as high as 1200°C along the length of the test beam. The hot junction of the thin film thermocouple was placed inside the hot zone of a tube furnace, a heat shield was placed just outside the hot zone and the cold junction was clamped to an aluminum cooling block just outside the furnace. The aluminum block was cooled with room temperature water to maintain the cold junction temperature during thermal cycling of the furnace. Additional insulation of the cold junction was provided by high temperature packing material. The custom tube furnace rig for thermocouple testing is shown in panels of figure 7. This testing rig effectively placed a temperature difference, from 0°C to 1200°C, along the length of the 7” beam, which could be controlled by altering the 8” hot zone temperature of the furnace. The hot and cold junction temperatures were monitored with commercial type-S and type-K wire thermocouples, respectively, to continuously measure the temperature difference along the beam. The thermoelectric voltage of each thin film thermocouple was collected using a data acquisition system by attaching copper extension wires to the platinum bond pads of each thermocouple using a conductive silver paste.

The thermoelectric properties of thermocouple library elements fabricated using combinatorial chemistry were tested using a hot probe method. A temperature

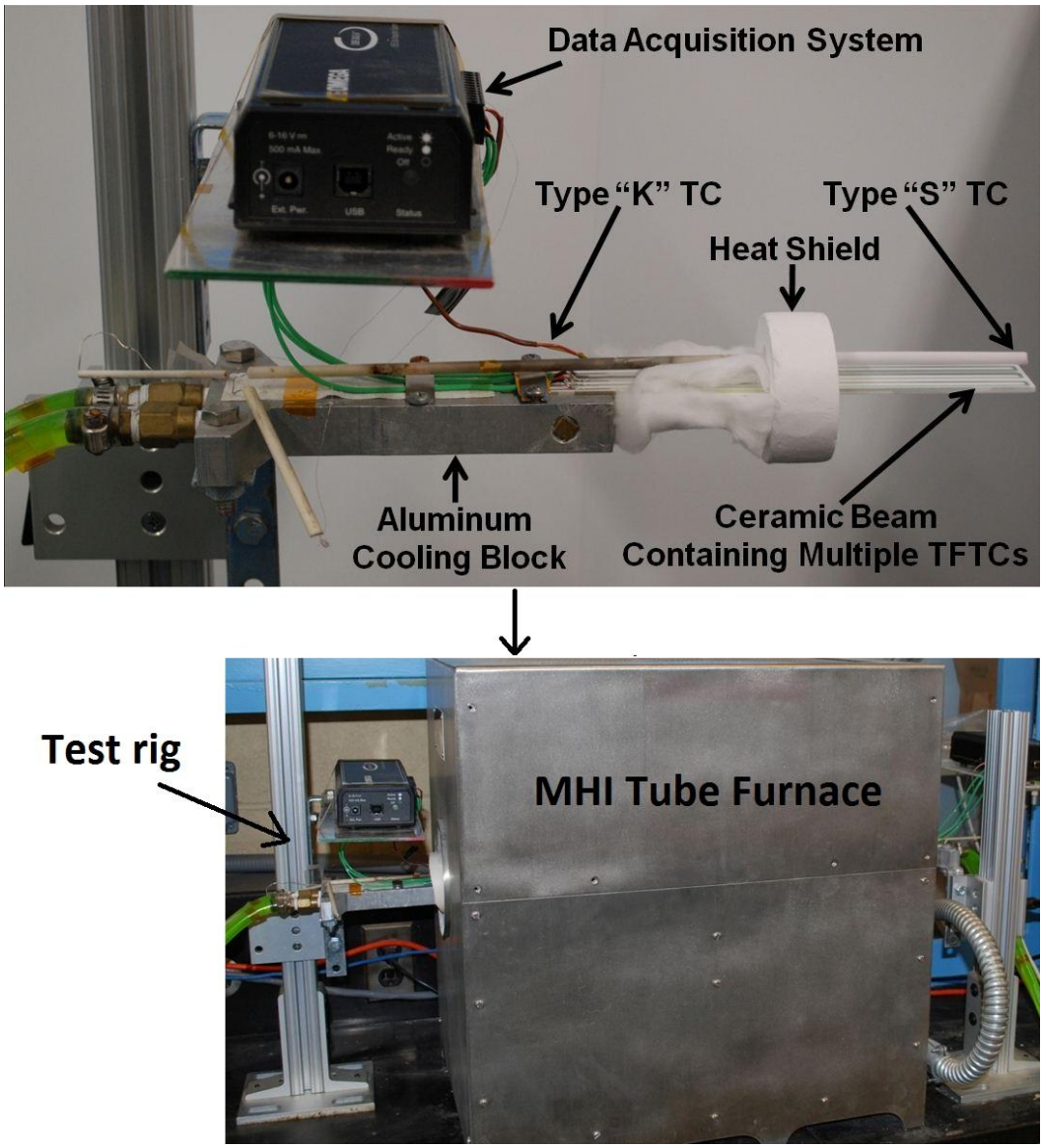

Figure 7. Custom tube furnace testing rig for thin film thermocouples deposited on ceramic beams, which applied a horizontal temperature difference along the length of the thermocouple measured with type-K and type-S wire thermocouples. This setup simulated the severe temperature gradients on the surface of components inside gas turbine engine hot sections.

difference of several degrees Celsius was placed along the length of the approximately centimeter long thermocouples by applying a hot probe at the hot junction of the thermocouple and letting the cold junction cool in air at room temperature. The thermoelectric voltage of each thermocouple was measured using the same data acquisition system as the tube furnace rig. Figure 8 shows the thermocouple library with probes applied to the thermocouples being tested (hot probe not shown). The area between the two probed thermocouples would be the location of the hot probe used to apply a temperature difference. Additionally, the electrical resistivity of each thermocouple is computed by measuring the thickness (each has constant area) using surface profilometry and resistance using a multimeter.

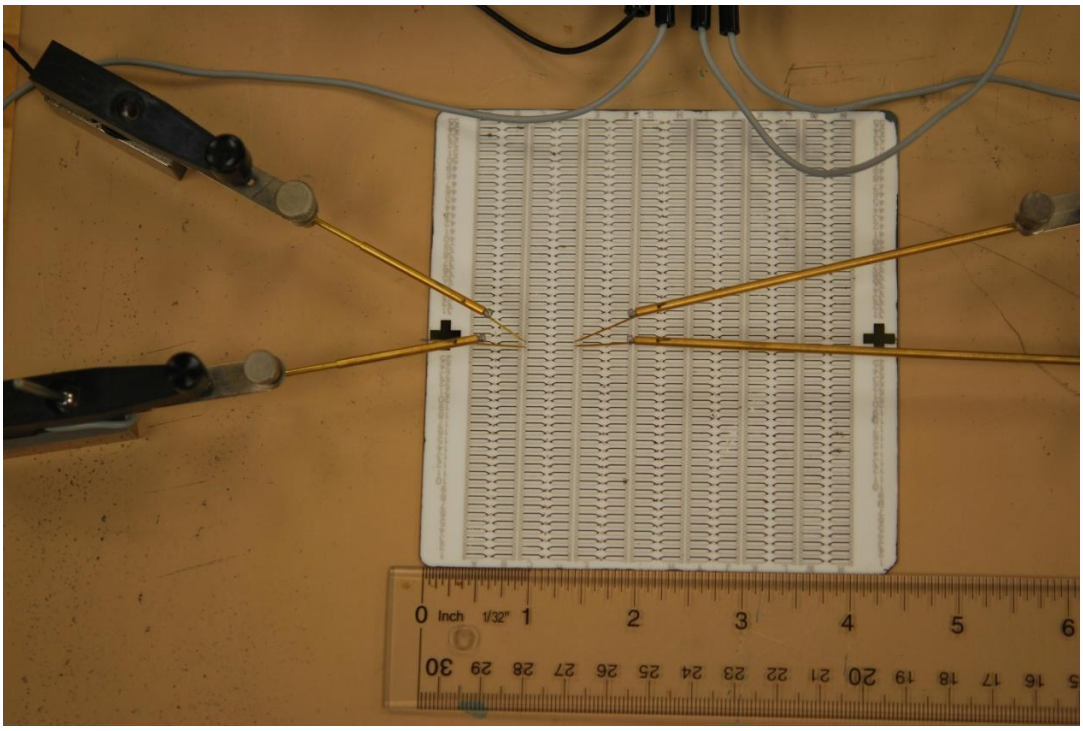

Figure 8. Combinatorial library thermocouples being tested for thermoelectric properties. A hot probe was positioned at the hot junction of each thermocouple to apply a temperature difference along its length and the thermoelectric voltage was recorded. Hot probe not shown in image.

CHAPTER 2

*STABILITY AND MICROSTRUCTURE OF INDIUM TIN OXYNITRIDE THIN FILMS

2.1 Abstract

Indium oxide (In_2O_3) and indium tin oxide (ITO) thin films have been investigated for high temperature thermocouple and strain gauge applications. Reactive sputtering in nitrogen-rich plasmas was used to improve the high temperature stability of indium oxide-based films in air and scanning electron microscopy was used to follow the microstructural changes in the nitrogen-processed films. When thermally cycled at temperatures above 800°C, a partially sintered microstructure comprised of nanometer-sized crystallites was revealed. A densified layer was also formed on the surface, which acted as an oxygen-diffusion barrier in the bulk film. This combined with a network of partially sintered oxynitride crystallites lead to considerable open porosity and a stabilizing effect on the ensuing electrical properties. In this article, the thermoelectric properties of nitrogen-processed films were evaluated at temperatures up to 1400°C. To study the effect of nitrogen plasma processing on the sintering kinetics and associated densification, the constrained sintering of the resulting films was followed as a function of time and temperature. Based on the measured thermoelectric properties of the nitrogen processed films, drift rates on the same order of magnitude as commercial type K wire thermocouples were realized for these all-ceramic thermocouples.

*Gregory, Amani, Tougas, and Drehman, *J. Am. Ceram. Soc.*, **95** [2], 705-710 (2012).

2.2 Introduction

Surface temperatures as high as 1500°C have been estimated for hot section components in modern gas turbine engines, and when combined with the severe thermal gradients often observed in these environments, modeling and simulation of the thermo-mechanical behavior of these components becomes very difficult. Therefore, direct temperature measurements are often necessary and thin film thermocouples, in particular, offer a significant advantage over wire thermocouples in such applications. Wire thermocouples are difficult to use for these measurements, since they cannot be easily incorporated onto the surfaces of thermal barrier coatings (TBC) deposited onto turbine blades, without affecting gas flow patterns.[1] Thin film thermocouples on the other hand can be directly deposited onto the surface of components without the need for adhesives or surface preparation which can alter the properties of the blades.[2] Furthermore, thin films add negligible mass (micrograms) to smaller turbine blades (grams) and have very fast response times (less than 1 μs).[3] However, the materials used in traditional metallic thermocouples, including those based on platinum and rhodium, suffer from reliability issues at temperatures above 900°C, such as selective rhodium oxidation. At these temperatures, the films are susceptible to a variety of problems including selective rhodium oxidation, which can cause the output of these devices to drift due to changes in composition. Furthermore, this can result in thinning and poor adhesion due to dewetting of the film-to-oxide surfaces. Platinum rhodium-based thermocouples also have very low output (on the order of 12 μV/°C) and the output can be affected by the catalytic nature of platinum

in the presence of certain hydrocarbons, leading to measurement errors as large as 50°C.[4,5]

Due to the limitations of platinum and platinum:rhodium thermocouples, several researchers have considered alternative materials for temperature measurement in harsh environments. Studies using TiC–TaC thin film thermocouples by Bhatt et al.[6] yielded some promising results at temperatures as high as 1080°C however; these devices were limited to operation in inert atmospheres or under vacuum conditions. Devices based on $MoSi_2$ and $TiSi_2$ films have shown promise in air at temperatures as high as 1200°C. The formation of a natural oxide with parabolic growth kinetics over these silicide films protects them to very high temperatures, which is essential due to the volatile nature of MoO_3.[7] However, to compensate for the loss of Si during oxidation, an extra layer of Si must be deposited under the thermo-element. With the added compensating layers, $MoSi_2$ films were stable enough to be considered for RTD applications. Unfortunately, the output of both silicide- and carbide-based thermocouples is low, even compared to type S thermocouples.

Commonly used as transparent conducting electrodes in many electronic and optoelectronic applications, In_2O_3 and In_2O_3:SnO_2 (ITO) are wide band gap, oxide semiconductors. At low concentrations of extrinsic dopants, charge carriers in these transparent conducting oxides are usually attributed to oxygen vacancy defects according to Eq. (1) below,

$$O_0^x \rightarrow 1/2O_2 + V_O^{\cdot\cdot} + 2e^{-1} \tag{1}$$

where $O_0^x \rightarrow 1/2O_2 + V_O^{\cdot\cdot} + 2e^{-1}$ are doubly charged oxygen vacancies. Tin-doping of In_2O_3 films has been used to dramatically improve the electrical conductivity, where

the substitution of two tin atoms and oxygen interstitial form a charge neutral carrier site, in addition to self-doping caused by intrinsic defects. Since grain boundaries act as impurity sinks, they play a critical role in the electrical conduction mechanism in these films. Therefore, any changes in the grain boundary area per unit volume due to sintering in these semiconductors will result in changes in the charge carrier concentration and will eventually lead to drift.[8]

Aperathitis et al.[9] have deposited films of indium oxynitride (InON) and indium tin oxynitride (ITON) by reactively sputtering from oxide targets in Ar/N_2 plasmas for optoelectronic applications. They concluded that increasing nitrogen content in the plasma reduces the transparency and the carrier concentration in these films. The ITON films have also been used for very high temperature thin film strain gauges,[10] which exhibited excellent piezoresistive response and very low drift rates at temperatures above 1500°C. Recently, we demonstrated a stable, all-ceramic thermocouple with a maximum operating temperature of 1250°C and an average Seebeck coefficient of 170 μV/°C, which is more than an order of magnitude higher than the output associated with metallic thermocouples that operate in the same temperature range.[11] In this study, thin film thermocouples were produced by reactive sputtering from In_2O_3 and ITO targets in a nitrogen rich plasma, which dramatically improved the stability, as indicated by the reduced hysteresis (upon heating/cooling) and drift rates of these thermocouples at temperatures approaching 1400°C. The effect of reactive sputtering on the stability of these films was monitored by measuring the thermoelectric response, electrical resistivity, and the densification or shrinkage of the film as a function of time and temperature.

2.3 Experimental Procedure

Thin film ceramic thermocouples were deposited by r.f. sputtering onto 190 mm 9 25 mm alumina substrates from In_2O_3, 95 wt% In_2O_3, 5 wt% SnO_2 (ITO 95-5), and 90 wt% In_2O_3, 10 wt% SnO_2 (ITO 90-10) targets (Umicore Indium Products, Providence, RI). The films were deposited using a MRC model 8667 and a MRC model 822 sputtering system, where a total gas pressure of 1.33 Pa was maintained during film deposition. The films were patterned by using conventional photolithography techniques whereby windows were formed in a negative photoresist, which have been used to pattern non-planar substrates such as turbine blades, and thus all depositions were performed at room temperature. Platinum bond pads and reference electrodes were sputtered from a high purity (99.99%) 100 mm diameter platinum target at an r.f. power of 300 W, resulting in 1.5 μm thick films. All thermoelectric testing done at temperatures in excess of 1200°C was performed using platinum ink to form the hot junctions instead of platinum films, due to dewetting of platinum under these conditions. All oxide films were deposited using the sputtering parameters shown in Table 1 and had nominal thicknesses of 10–12 μm. Prior to sputtering, a background pressure of less than 1×10^{-4} Pa was maintained in the vacuum chamber, the respective targets were pre-sputtered onto shutters for 10 min to remove surface contamination and release adsorbed water.

The thin film thermocouples were annealed at 500°C for 5 h in nitrogen, followed by a second 2 h anneal at 1200°C. During testing in air, one end of the thermocouples was placed into the hot zone of a tube furnace, to apply a temperature difference along the length of the substrate. The temperature at the cold junction was

Sputtering parameters	Pt	In_2O_3	InON	ITON 95/5	ITON 90/10
Target diameter (mm)	100	150	150	125	150
Power (W)	300	350	350	350	350
Power density (W/cm^2)	3.85	1.98	1.98	2.85	1.98
Sputtering gas pressure (Pa)	Ar: 1.33Pa	Ar: 1.33 Pa	Ar: 1.07 Pa N_2: 0.27 Pa	Ar: 1.07 Pa N_2: 0.27 Pa	Ar: 1.07 Pa N_2: 0.27 Pa
Deposition rate (μm/hr)	0.6	1.2	1.1	0.9	1.4
Film thickness (μm)	1.5	10.0 to 12.0	10.0 to 12.0	10.0 to 12.0	10.0 to 12.0

Table 1. Sputtering conditions of platinum, indium oxide and ITO films.

maintained at 20°C using an ethylene glycol coolant circulated through an aluminum cooling block connected to a chiller. Both the hot and cold junction temperatures were continuously monitored using type S and type K thermocouples, respectively. The furnace was thermally cycled from room temperature to 1400°C at a heating/cooling rate of 3°C/min. Long-term stability tests of the thermocouples were obtained by testing the thermocouples for 200 h across a thermal difference of 1200°C. The temperature coefficient of resistivity of the oxide and oxynitride films was determined using the van der Pauw method. The sintering and growth kinetics of In_2O_3 films sputtered in varying argon, oxygen and nitrogen partial pressures was measured using a Dektak surface profilometer to determine the change in thickness of films, deposited on highly polished alumina wafers as a function of time and temperature. These oxide films were also grown on sapphire substrates and characterized using with grazing incidence X-ray diffraction (GI-XRD) utilizing a $Cu_{K\alpha}$ radiation source.

2.4 Results and Discussion

The Seebeck coefficient in both degenerate and non-degenerate semiconductors is highly dependent on the charge carrier concentration, N_D.[8] To fabricate thermocouples with low drift rates, variations in N_D must be minimized. As grain boundaries act as impurity sinks, they play a critical role in the conduction mechanism associated with transparent conducting oxides such as ITO.[8] To obtain stable thermoelectric responses, all thermocouples were heat-treated in N_2 for 5 h at 500°C to eliminate point defects in the films, such as trapped argon and to improve the electrical conductivity. Because the cold junction of the thermocouple is never

exposed to the peak operating temperatures of the device, inhomogeneities in the film caused by compensation of oxygen vacancies in the hot junction can lead to noise, drift and even voltage spikes. These were eliminated by heating the entire thermocouple for 2 h in air at 1200°C. However, heat treatments cannot reduce drift in the Seebeck coefficient caused by sintering of the materials in the hot junction. Therefore, reduced sintering kinetics and oxygen diffusion barriers were employed to improve the long-term performance of these ceramic thermocouples.

As nitride ceramics exhibit much slower sintering kinetics compared to oxide ceramics,[10] oxynitride thermoelements were prepared by reactively sputtering in nitrogen-rich plasmas from In_2O_3 and ITO targets. This technique has been described in the literature for ITO films heat-treated under various nitrogen partial pressures and can lead to significant nitrogen incorporation into the films as well as a reduction in the optical band gap and carrier concentration.[12] Figure 9 shows the microstructure of thermally cycled InON and In_2O_3 films. A network of submicrometer pores, capped with a densified oxynitride layer was observed in the nitrogen processed films [Fig. 9(b)] which was not evident in the densified Ar processed film [Fig. 9(d)]. When InON films were grown on a sapphire substrate (Fig. 10), relatively large (2–5 μm) faceted crystallites were formed over a network of submicrometer grains. While this also occurred to a lesser extent in InON films prepared on alumina substrates, these features were only observed on the surface of the InON films and were not present in any of the tin doped samples. The X-ray diffraction patterns of the In_2O_3-based films grown on sapphire are shown in Fig. 11. When the In_2O_3 films were prepared in pure argon, the (400) peak dominated the XRD pattern, suggesting that the films are highly

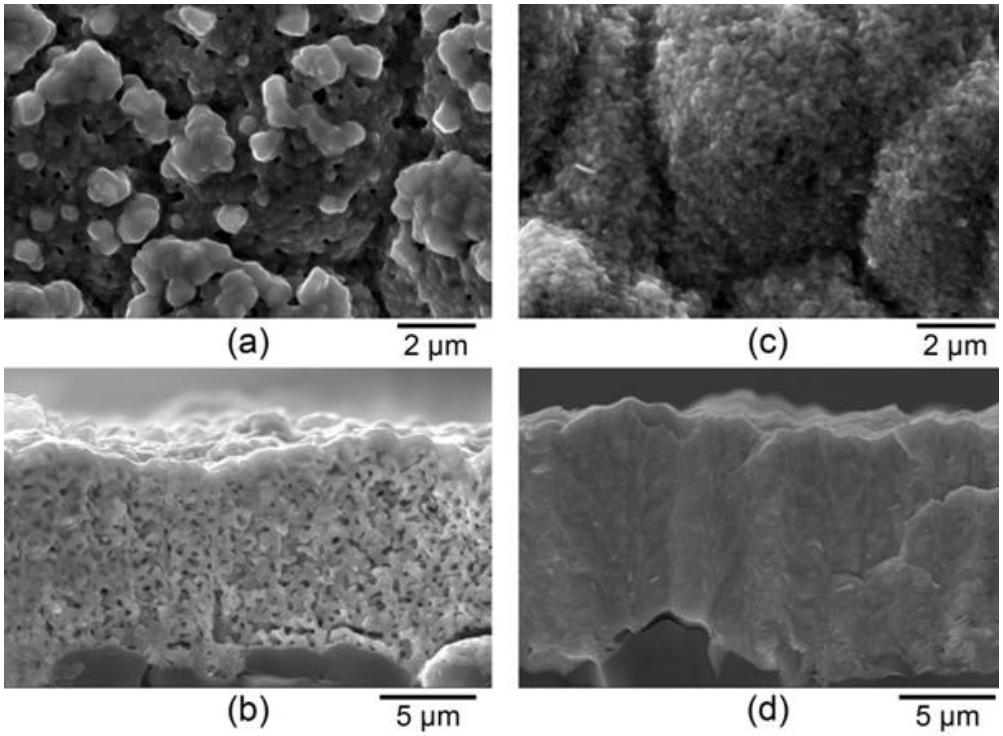

Figure 9. SEM micrographs of (a) InON film (b) fracture surface, (c) In_2O_3 film and (d) fracture surface on compact alumina after annealing in air at 1250°C for ten hours. Note the dense layer formed on the surface of the InON film and the porosity contained beneath (b). The In_2O_3 film (d) had less porosity than the InON film.

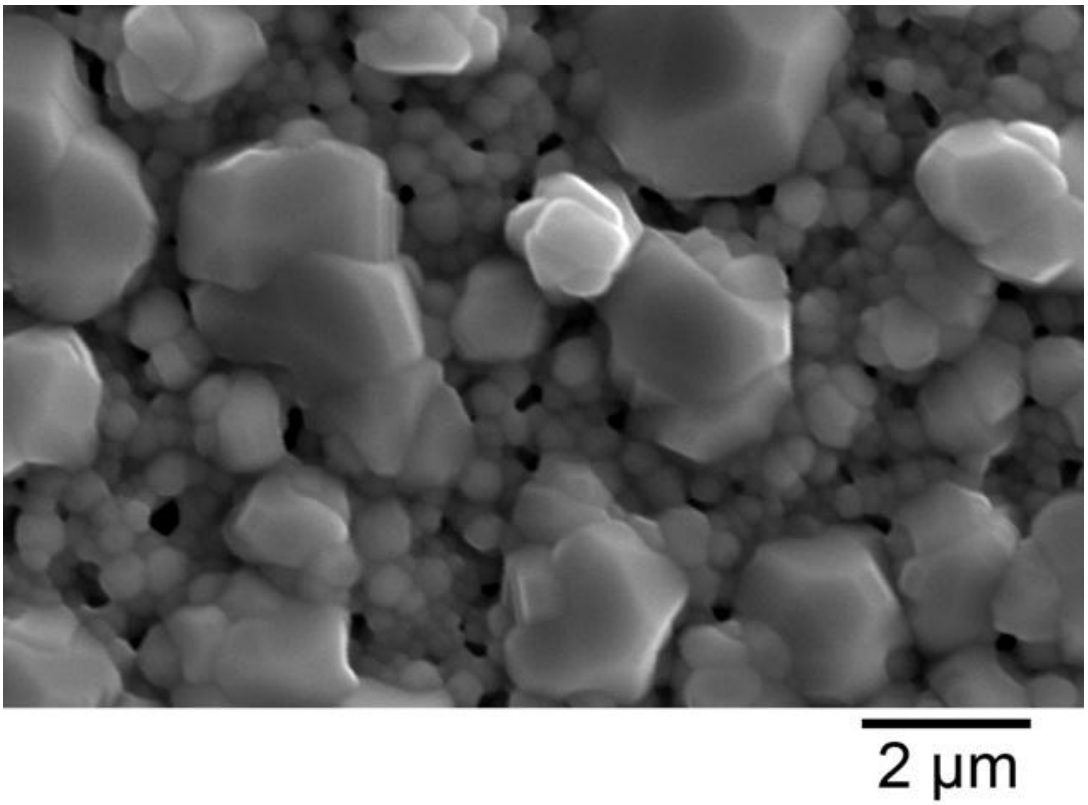

Figure 10. SEM micrograph of InON film prepared on c-axis sapphire after annealing in air at 1250°C for ten hours. Note the faceted particles and porosity. Less porosity is seen here relative to the fracture surface of the same film (Figure 9b).

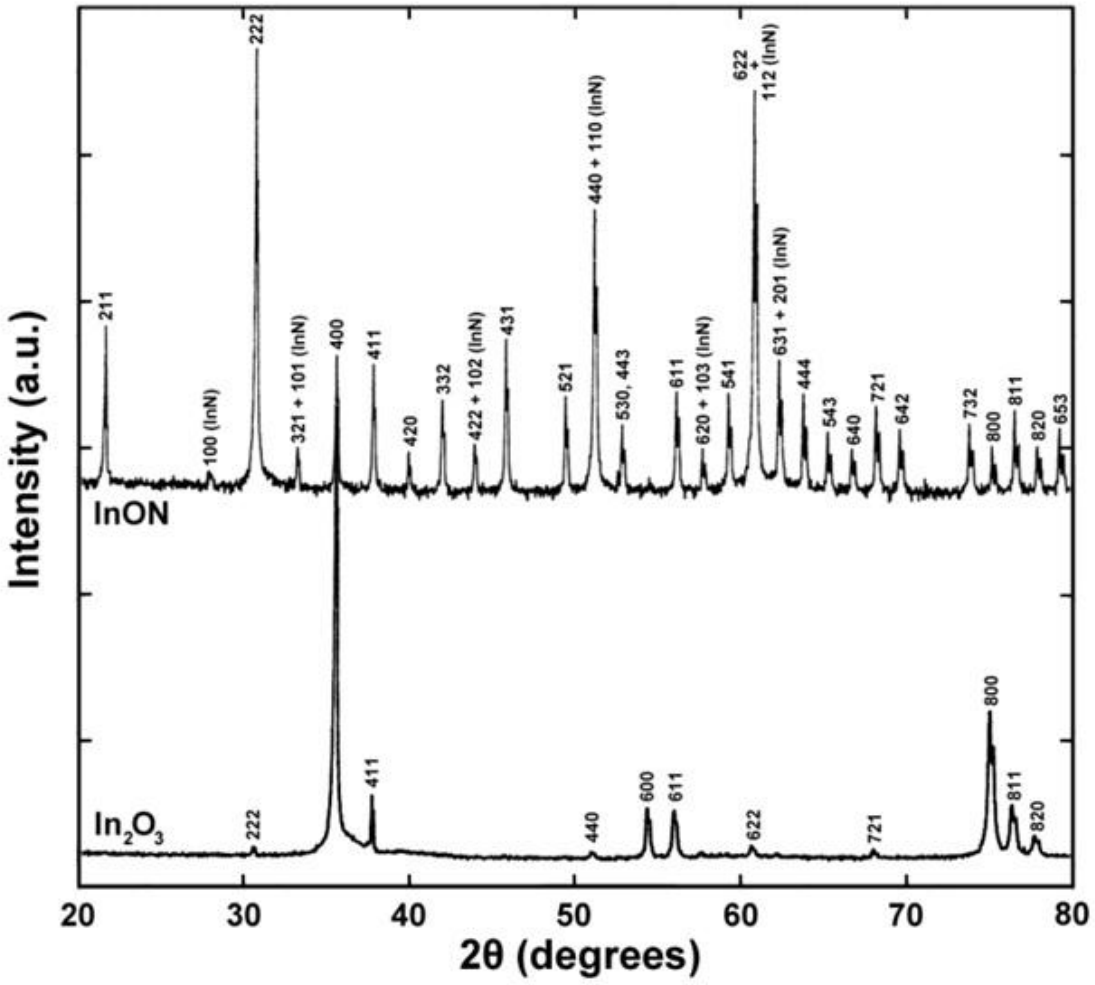

Figure 11. X-ray diffraction patterns of In_2O_3 and InON films after annealing in air at 1250°C for ten hours. Peaks corresponding to In_2O_3 and InN were present in the InON film indicating that metastable nitrogen was retained in the film as part of a indium nitride phase.

oriented. In the nitrogen-processed films, XRD peaks corresponding to both In_2O_3 and InN were identified, and no preferred orientation was observed in these films. We believe that the isolated crystallites observed on the surface were formed by a vaporization–condensation mechanism, whereby the growth of InON was triggered by the instability of sub-oxides of indium at low temperatures and oxygen-partial pressures.[13] This led to the formation of a densified, nonporous layer that can be seen in the SEM fractographs in Fig. 9(b). A slight increase in the lattice spacing was also observed in the InON films relative to the In_2O_3 films. A shift of 2.530 to 2.546 Å was calculated for the (400) peak in these films. This shift has been previously documented for ITON and other oxynitrides,[9,14] and suggests that nitrogen was present in the "bulk" film as well as in the densified layer.

Studies performed on the rapid heating of ITO ceramics by Kim et al. suggest that rapid densification of the surface grains constrains the sintering in the bulk material.[15] It is believed that the nitrogen incorporated into the film during sputtering was metastably retained and trapped in the pores and grain boundaries in the film. Upon heating in air, the reduced sintering kinetics and oxygen diffusion into grains resulted in pore growth and expansion, a phenomenon which has been previously observed in the sintering of submicrometer Si powders and in several oxides including MgO, ZnO, and SnO_2.[16,17] The constrained volume shrinkage ($[V_0 - V]/V_0$) and sintering, which was first investigated by Garino and Bowen, was monitored as a function of time at temperature.[18] Figure 12 shows the results from the constrained sintering of In_2O_3 films at 1300°C and the associated effect of different sputtering gasses on densification. In the more stoichiometric In_2O_3 films (prepared in Ar/O_2

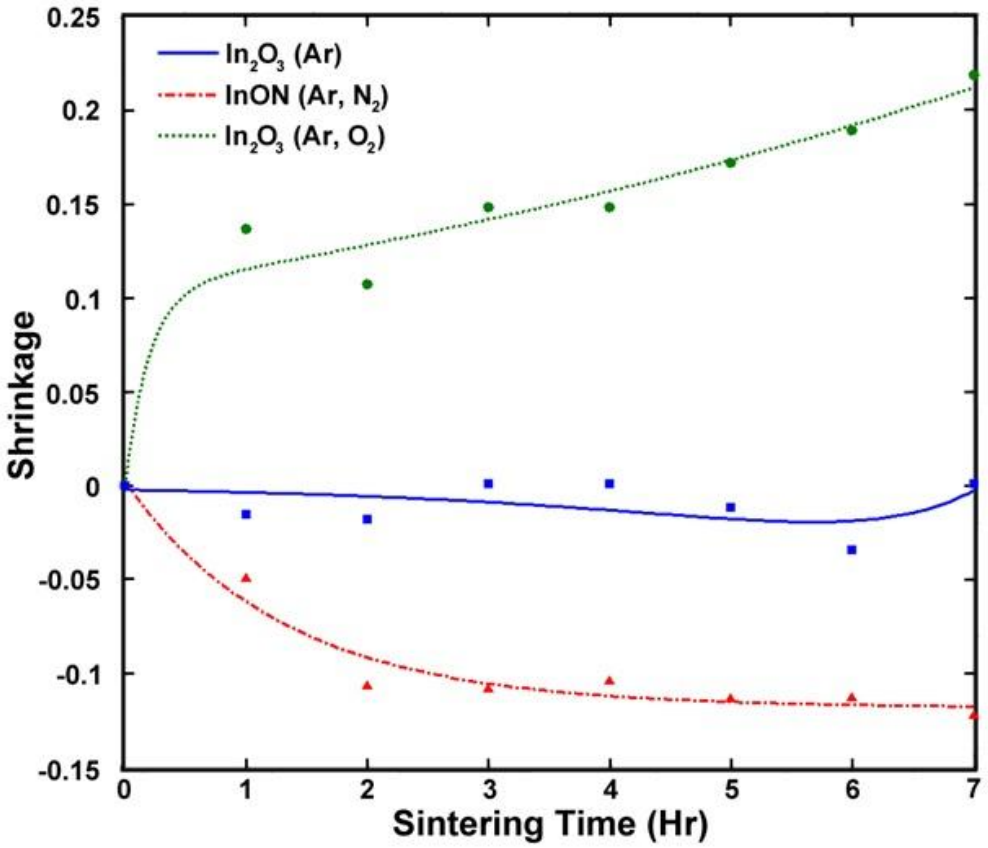

Figure 12. Isothermal constrained shrinkage ($(V_0-V)/V_0$) of In_2O_3 films prepared in Ar (blue square), Ar/O_2 (green circle) and Ar/N_2 (red triangle) plasmas at 1300°C as a function of time.

plasmas), sublimation was observed during heat treatments after rapid densification, while no significant thickness changes were observed in films prepared in argon plasmas. On the other hand, a 12% increase in volume was observed in the oxynitride film after 2 h at temperature, consistent with a pore growth mechanism during sintering.[17]

Prior to heat treatment in air, the In_2O_3 and ITO films behave like degenerate semiconductors due to the very high concentration of defects in the film. After the material had been heated in air, thermally activated oxygen diffusion resulted in partial compensation of the doubly charged oxygen vacancies in the film. However, thermally cycled In_2O_3 films remain relatively conductive at room temperature (with resistivities as low as 0.02 Ω·cm) despite the compensated charge carriers. This is a result of the film's complex bixbyite crystal structure which contains unoccupied oxygen interstitial positions.[19] The temperature dependence of the electrical resistivity in ITO films after heat treatments in air has been well documented and is known to have a distinct transition corresponding to the excitation of all dopant species to the conduction band, which occurs at temperatures between 600°C and 700°C.[20] Thermally activated electrical conductivity was observed in these semiconductors and is described by the following equation:

$$\sigma = \sigma_0 \exp\left(-\Delta E_a / kT\right) \tag{2}$$

where k is Boltzmann's constant, T is the absolute temperature, and ΔE_a is the activation energy, which is the energy gap between the conduction band edge and the Fermi level. Arrhenius plots showing the electrical conductivity and activation energy of both argon and nitrogen processed In_2O_3 and ITO films are displayed in Fig. 13.

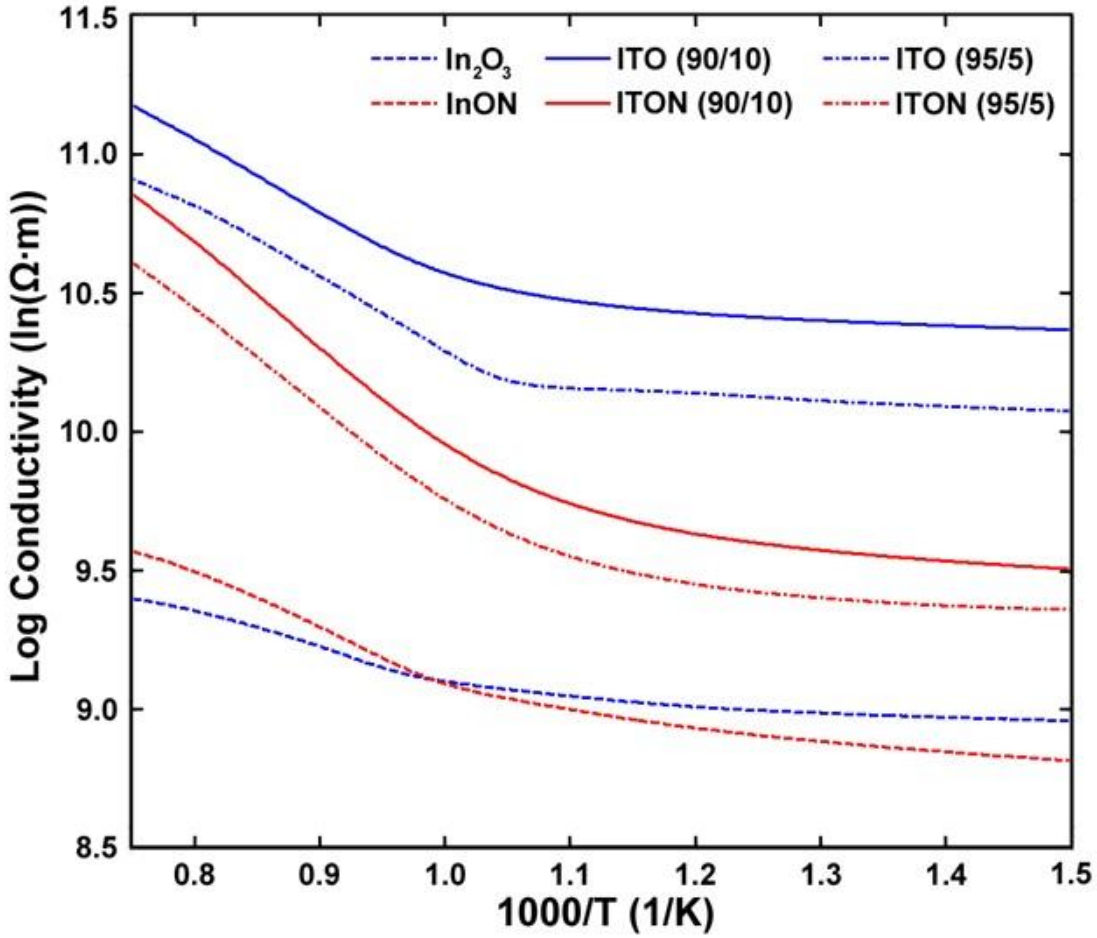

Figure 13. Electrical resistivity of In_2O_3 and ITO films prepared in Ar and Ar/N_2 plasmas.

The activation energies corresponding to temperatures above and below the transition temperature are listed in Table 2. These results indicate that the oxynitride films have significantly higher activation energies (~70% increase) than their oxide counterparts, supporting the XRD results, that nitrogen is present in the bulk film, as well in the densified layer. Nitrogen acts as a valence band acceptor in oxide semiconductors and incorporation of nitrogen into the films results in a reduction of the Fermi energy, which explains the shift in activation energy. In all cases, the oxynitride films were more resistive than their oxide counterparts when measured at room temperature.

To investigate the effects of reactive sputtering on the thermoelectric power of In_2O_3, several thermocouples were prepared in various argon, oxygen and nitrogen partial pressures. These thermocouples were tested relative to platinum reference electrodes, as shown in Fig. 14. Here, it was found that the films prepared in pure argon and in oxygen rich plasmas had larger magnitude Seebeck coefficients than those deposited in nitrogen-rich plasmas. For non-degenerate semiconductors such as In_2O_3, the Seebeck coefficient described by,

$$S(N_D) = -\frac{Ak}{e} - \frac{k}{e}\ln\left(\frac{(2\pi m_e^* kT)^{2/3}}{\hbar^3 N_D}\right) \quad (3)$$

where S is Seebeck, k is the Boltzmann constant, e is the electron charge, m_e^* is the effective mass, $\hbar$ is Planck's constant, and A is a transport constant (typically $0 \leq A \leq 4$).[21] For non-degenerate semiconductors, a decrease in the carrier concentration increases the magnitude of the Seebeck coefficient. It is expected that the oxynitride films will have a significantly reduced Seebeck coefficient since nitrogen acts as a valence band acceptor in conducting oxides, making the thermoelectric power more

Target Material	Oxide Film		Oxynitride Film	
	T < 950 K	T > 950 K	T < 950 K	T > 950 K
In_2O_3	5.86 meV	115 meV	8.68 meV	169 meV
ITO 95/5	16.1 meV	205 meV	25.1 meV	313.8 meV
ITO 90/10	13.5 meV	212 meV	21.3 meV	286 meV

Table 2. Activation energies associated with the electrical conductivities of various oxide and oxynitride films as a function of thermal cycling.

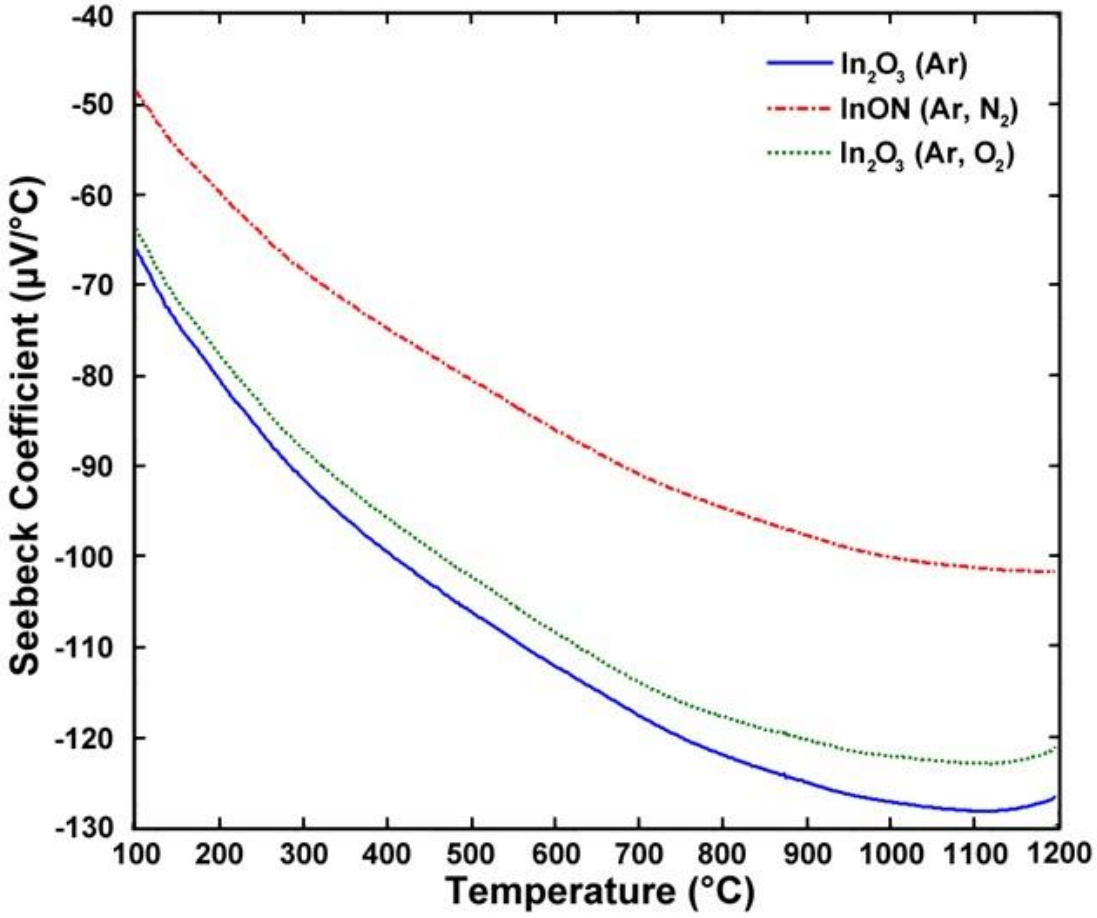

Figure 14. Seebeck coefficient of In_2O_3 films prepared in Ar, Ar/N_2, and Ar/O_2 plasmas.

positive (smaller magnitude). The Seebeck coefficient of ITO on the other hand is given by,

$$S(N_D) = -\left(\frac{\pi}{3N_D}\right)^{2/3} \frac{8k^2 m^* T}{3e\hbar^2}\left(A + \frac{3}{2}\right) \tag{4}$$

which is identical to the expression used for metals and is valid because the free electron-like behavior observed in degenerate semiconductors, where *A* is a transport constant that describes the predominant scattering process.[8] Incorporation of nitrogen into ITO has been shown to cause a reduction in carrier concentration as well as the Fermi level due to an increase in activation energy and will therefore increase the Seebeck coefficient of ITO.[11] In the In_2O_3–ITO thermocouples fabricated by Chen et al.,[11] a degenerately doped n-type semiconductor with a very low Seebeck coefficient was combined with a non-degenerate n-type semiconductor having a relatively high Seebeck coefficient, which yielded thermoelectric powers greater than 150 μV/°C. During the lifetime of these devices, significant changes in the microstructure were observed, which led to large drift rates, which is defined according to Eq. (5) as,

$$DR(T) = \frac{\Delta V(T)}{V(T)_{Ref}} \cdot \frac{T}{\Delta t} \tag{5}$$

By introducing nitrogen into the films, the thermoelectric powers of the non-degenerate material were reduced and those of the degenerate material were increased. This resulted in a reduction in the overall Seebeck coefficient of the oxynitride based thermocouples. However, despite their lower thermoelectric output, the oxynitride thermocouples had lower drift rates (Table 3). The long-term stability of these thin film thermocouples was compared by computing their drift rates after 200 h of testing

Thermocouple Pair	$V(\Delta T) = A(\Delta T)^3 + B(\Delta T)^2 + C(\Delta T)$			Seebeck Coefficient at 1200°C (μV/°C)	Drift Rate (°C/hr)
	A ($mV/°C^3$)	B ($mV/°C^2$)	C (mV/°C)		
In_2O_3 vs. ITO (95/5)	-6.90×10^{-7}	1.44×10^{-4}	7.27×10^{-2}	170	3.76
In_2O_3 vs. ITO (90/10)	-7.78×10^{-7}	1.41×10^{-4}	6.33×10^{-2}	162	20.4
InON vs. ITON (95/5)	-1.43×10^{-8}	4.66×10^{-5}	2.17×10^{-2}	68	0.57
InON vs. ITON (90/10)	-1.61×10^{-8}	5.47×10^{-5}	2.54×10^{-2}	56	0.63

Table 3. Thermoelectric response and drift rate of In_2O_3 vs. ITO and InON vs. ITON thin film thermocouples.

at a hot junction temperature of 1200°C. For comparison, a 0.5 mm diameter type K wire thermocouple had a drift rate of 0.18 K/h at operating temperatures of 1100°C.[22] Furthermore, the hysteresis in the thermoelectric output observed during rapid heating and cooling cycles of the ceramic thermocouples (Fig. 15) was further reduced through nitrogen processing. At temperatures above 1400°C, a loss of tin in the ITON films was observed, ultimately resulting in device failure. However, the nitrogen-processed InON films survive temperatures greater than 1500°C. The significant improvements observed in the stability and hysteresis of the InON versus ITON thermocouples make them much more suitable for high temperature measurements, despite their relatively small thermoelectric outputs.

2.5 Conclusion

Ceramic thermocouples based on porous indium oxynitride and indium tin oxynitride thin films were developed to replace noble metal thermocouples used to measure temperatures in the hot section of gas turbine engines. Metastably retained nitrogen was introduced into the films by reactive sputtering in nitrogen-rich plasmas where, upon heating, the nitrogen becomes trapped in isolated pores with grain boundaries affecting the solid/vapor equilibrium. Due to the reduced sintering kinetics of nitride ceramics relative to oxide ceramics, the grain boundaries were stabilized to very high temperatures. Since the Seebeck coefficient for both nondegenerate and degenerate semiconductors is a function of the charge carrier concentration, a significant reduction in the drift rate was observed for these oxynitride-based thermocouples compared to thermocouples prepared in argon plasmas.

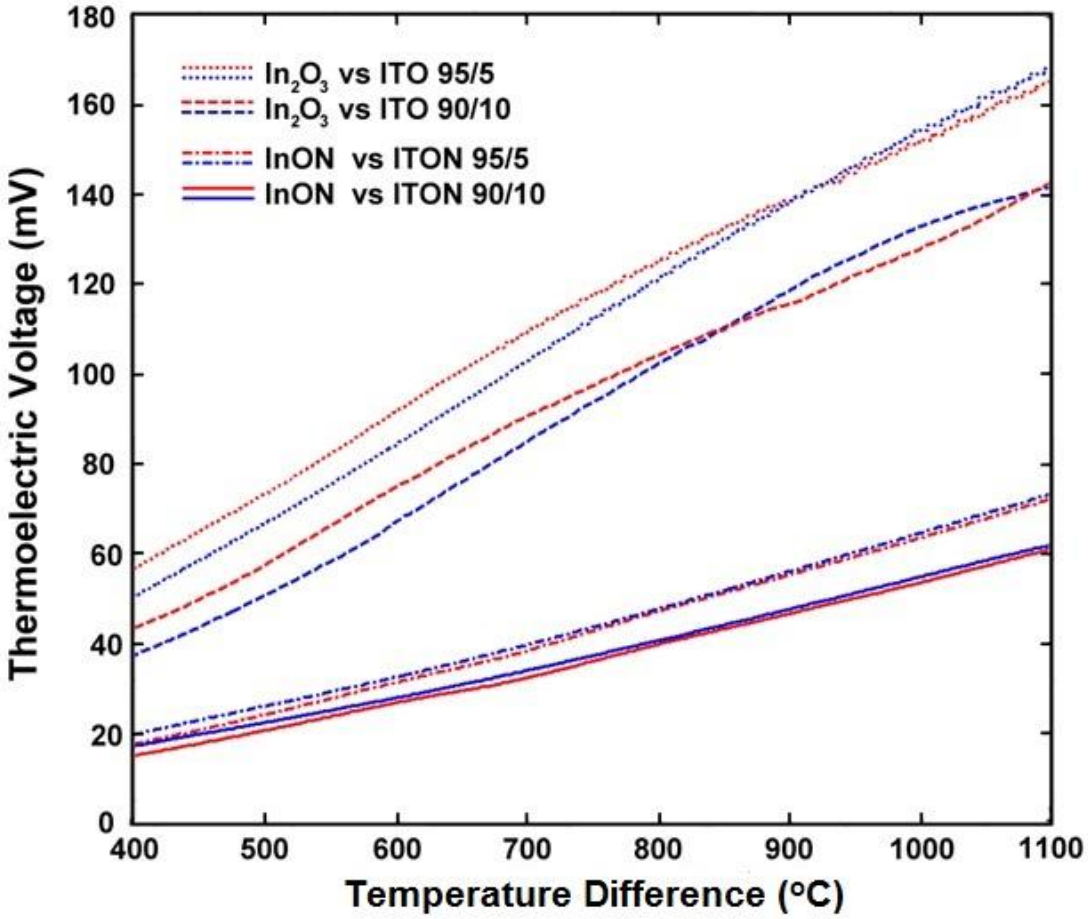

Figure 15. Thermoelectric output and hysteresis (heating: red, cooling: blue) of ceramic thin film thermocouples.

List of References

[1]J. F. Lei and H. A. Will, "Thin-Film Thermocouples and Strain-Gauge Technologies for Engine Applications", Sensors and Actuators A, 65 (1998) 187-193.

[2]L. C. Martin and R. Holanda, “Applications of Thin Film Thermocouples for Surface Temperature Measurement”, NASA TM-106714, (1994).

[3]H. Choi and X. Li, "Fabrication and application of micro thin film thermocouples for transient temperature measurement in nanosecond pulsed laser micromachining of nickel", Sensors and Actuators A, 136 (2007) 118-124.

[4]G. E. Aniolek and O. J. Gregory, "Thin film thermocouples for advanced ceramic gas turbine engines", Surface and Coatings Technology, 68-69 (1994) 70-75.

[5]K. G. Kreider, "Sputtered high temperature thin film thermocouples", Journal of Vacuum Science Technology, 11 (1993) 1401-1405.

[6]K. Ellmer and R. Mientus, “Carrier transport in polycrystalline ITO and ZnO:Al II: The influence of grain barriers and boundaries”, Thin Solid Films, 516 (2008) 5829-5835.

[7]E. Aperathitis, M. Bender, V. Cimalla, G. Ecke, and M. Modreanu, “Properties of rf-sputtered indium-tin-oxynitride thin films”, Journal of Applied Physics, 94 (2003) [2]

[8]O.J. Gregory and T. You, “Piezoresistive Properties of ITO Strain Sensors Prepared with Controlled Nanoporosity”, Journal of the Electrochemical Society, 151 (2004) (8) H198-H203

[9]X. Chen, O.J. Gregory, and M. Amani, “Thin-Film Thermocouples Based on the System In_2O_3-SnO_2”, Journal of the American Ceramic Society, 94 (2011) [3] 854-860

[10]E. Aperathitis, M. Modreanu, M. Bender, V. Cimalla, G. Ecke, M. Androulidaki, and N. Pelekanos, “Optical characterization of indium-tin-oxynitride fabricated by RF-sputtering”, Thin Solid Films, 450 (2004) 101-104

[11]E. Medvedovski, C. J. Szepesi, O. Yankov, and P. Lippens, “Indium tin oxide nanosized transparent conductive thin films obtained by sputtering from large size planar and rotary targets”, Ceramic Transactions, 223 (2010) 125-146

[12]B. C. Kim, J. H. Lee, J. J. Kim, and T. Ikegami, “Rapid rate sintering of nanocrystalline indium tin oxide ceramics: particle size effect”, Materials Letters, 52 [1-2] (2002) 114-119

[13]O. J. Gregory, S. B. Lee, R. C. Flagan, “Reaction Sintering of Submicrometer Silicon Powder”, Journal of the American Ceramic Society, 70 (1987) [3] C52-C55

[14]J.A. Varela, O.J. Whittemore, E. Longo, “Pore size evolution during sintering of ceramic oxides”, Ceramics International, 16 (1990) [3] 177-189

[15]T. J. Garino and H. K. Bowen, “Kinetics of Constrained-Film Sintering”, Journal of the American Ceramic Society, 73 (1990) [2] 251-257

[16]S.P. Harvey, T.O. Mason, Y. Gassenbauer, R. Schafranek, and A. Klein, “Surface versus bulk electronic/defect structures of transparent conducting oxides: I. Indium oxide and ITO”, Journal of Physics D: Applied Physics, 39 (2006) 3959-3968

[17]O. J. Gregory, Q. Luo, and E. E. Crisman, "High Temperature Stability of Indium Tin Oxide Thin Films", Thin Solid Films, 406 (2002) 286-293.

[18]G. Jonker, “The Application of Combined Conductivity and Seebeck-Effect Plots for the Analysis of Semiconductor Properties”, Philips Research Report, 23 (1968) [2] 131-138

[19]R. E. Bentley, “Handbook of Temperature Measurement Vol. 3: Theory and Practice of Thermoelectric Thermometry”, Springer, 1998.

CHAPTER 3

*THERMOELECTRIC PROPERTIES AND MICROSTRUCTURE OF Cu-In-O THIN FILMS

3.1 Abstract

Combinatorial chemistry techniques were used to study the thermoelectric properties of sputtered thin films in the system copper oxide (CuO) and indium oxide (In_2O_3). Hundreds of thin film thermocouples or combinatorial library elements were simultaneously deposited, each with a unique spatially dependent chemistry. The resulting thermoelectric properties of each element were determined along with electrical resistivity as a function of composition. Energy dispersive spectroscopy was used to identify the composition of each thermo-element and electron and x-ray diffraction were used to determine the degree of crystallinity and phases present. Transmission electron microscopy was used to characterize the microstructure of selected thermo-elements. A change in sign of the thermoelectric voltage was observed in the thermo-element containing 40 atomic percent indium, which suggests a change in the dominant carrier type occurred, from p-type to n-type. Based on this finding, the fabrication of thermoelectric p-n junctions using the same base Cu-In-O semiconductor appears feasible.

*Gregory, Tougas, Amani, and Crisman, *J. Electron. Mater.*, in press (2013).

3.2 Introduction

Transparent conducting oxides (TCO) based on the material system Cu-In-O have been considered for applications such as flat panel displays, solar cells, and thin film transistors [1, 2]. However, there have been relatively few studies of the thermoelectric properties of such materials to date [3]. Recently, considerable efforts have focused on the thermoelectric properties of oxides for applications such as energy harvesting, and power generation [4-7]. Compared with more conventional thermoelectric materials, oxides offer dramatically improved chemical stability in air, inherently higher carrier concentrations, and can be used at significantly higher temperatures. Both, indium oxide (In_2O_3), an n-type semiconductor, and In_2O_3 doped with +4 cations has shown promise as a thermoelectric material [3, 4]. Copper oxide (CuO), a p-type semiconductor, has been considered for thermoelectric applications but has a relatively small band gap (1.2 eV) compared to In_2O_3 [8], which limits its use in high temperature thermoelectric applications. Furthermore, CuO changes oxidation state as a function of temperature [9, 10]. However, alloys comprised of CuO and In_2O_3 typically exhibit larger band gaps (on the order of 3eV) than the stand-alone materials, making them more suitable for thermoelectric applications.

The delafossite ($Cu^{+1}In^{+3}O_2$) phase in the Cu-In-O system has received considerable attention for TCO applications [11-13]. This material can be "tuned" in such a way that either p-type or n-type carriers can dominate; e.g. by substituting Sn^{+4} for indium or Ca^{+2} for copper [12, 14]. The formation of this phase, or this phase with the inclusion of dopants, requires careful processing routes. These routes have been demonstrated successfully in previous studies [14, 15]. However, few if any studies

have focused on tuning the composition of the Cu-In-O compounds to achieve p-type or n-type dominant carriers in the base compound without the need for doping.

In this study, combinatorial chemistry techniques were used to fabricate thin film thermo-elements based on Cu-In-O prepared by sputtering from CuO and In_2O_3 targets. By combining a p-type semiconductor (CuO) with an n-type semiconductor (In_2O_3), thin film thermo-elements with either p-type or n-type character could be produced without relying on synthesizing the p-type or n-type auto-doped $CuInO_2$ phase. The library thermo-elements were largely amorphous and each was catalogued according to the atomic percentage of indium in the film. The relation between the library element composition and the dominant carrier type was characterized using the hot probe method. A transition from p-type to n-type conduction in the Cu-In-O system was observed at a film composition of 40 at% indium. Energy dispersive spectroscopy (EDS) was used to determine the composition of each thermo-element and the microstructures of as-deposited and annealed thermo-elements were characterized using transmission electron microscopy (TEM). Electron diffraction in conjunction with TEM and x-ray diffraction (XRD) were used to determine the extent of crystallinity and the distribution of phases in select library thermo-elements.

3.3 Experimental Procedure

Cu-In-O films were deposited onto high purity alumina substrate and oxidized silicon wafer by co-sputtering from CuO and In_2O_3 targets to form a combinatorial library containing thermo-elements in the Cu-In-O system. Prior to deposition, reference electrodes (complementary thermocouple leg to Cu-In-O thermo-element)

were fabricated using photolithography in conjunction with lift-off. Platinum, sputtered in ultra high purity (UHP) argon at 9 mT, was deposited as the reference electrode material. A photolithographic step was used to create 770 Cu-In-O thermo-elements with each thermo-element at different position relative to the two sputtering targets. The sputtering targets were six inches in diameter and were spaced 27.3 cm apart. A radio frequency power of 200 W was fed continuously to each sputtering target during deposition. In this way, a chemical composition gradient was established in the thermo-elements along the axis between the targets and a thickness gradient was established in the orthogonal direction. The resulting thermocouples formed an array suitable for rapid thermoelectric property screening.

All thermocouples were subsequently annealed in nitrogen at 400°C for five hours to release trapped argon and densify the thermo-elements. Final film thicknesses ranged from 1 to 2 μm. Thermoelectric data were obtained from the library thermocouples deposited on an alumina substrate, after a temperature difference was established between the hot and cold junctions. Each thermo-element was typed p- or n- based on the voltage sign relative to the platinum reference electrode. Voltages were recorded using an iOTech USB data acquisition system and *Personal Daq View Plus*© software. Thin film type-K thermocouples were deposited, by sputtering from alumel and chromel targets in 9 mT Ar, at the hot and cold junction of a thermocouple with the same geometry as the library thermocouples to calibrate the temperature difference across the junction. Electrical resistivity was measured on films deposited on the oxidized surface of a silicon wafer after the thermocouples were nitrogen annealing. The composition of each thermo-element in the library array was

determined with EDS measurements on a JEOL-5900 SEM. The microstructures of select library thermo-elements were examined in a JEOL JEM-2100 TEM by depositing films directly onto silicon nitride grids. The thin films were examined as-deposited, after a 400 °C, 5 h nitrogen anneal, and after repeating the nitrogen anneal another 5 h at 400 °C. A Rigaku Ultima-IV XRD system was used to determine the degree of crystallinity and distribution of phases present in selected thermo-elements.

3.4 Results and Discussion

3.4.1 Thermoelectric Properties

The thermoelectric voltages of the Cu-In-O combinatorial library thermo-elements are summarized in Figure 16, which shows thermoelectric voltage as a function of position. By comparing the thermoelectric voltage and spatial distribution of the chemical composition, maps of thermoelectric voltage and resistivity as a function of composition were generated (Figure 17). Figure 17a shows a continuous transition from n- to p- conduction occurring at a film composition of 40 at% indium. The CuO-In_2O_3 phase regions were superimposed over the data in Figure 17a. It indicates that the n- to p- transition occurs in a copper rich film, which falls within a two phase region of CuO and $Cu_2In_2O_5$. Since the films studied are largely amorphous, we suggest that a doping effect from the copper was responsible for the observed p-type behavior in the copper rich films rather than from the formation of different phases in the material as the copper content was increased. Figure 17b indicates that little variation in the electrical resistivity was observed for thermo-elements containing

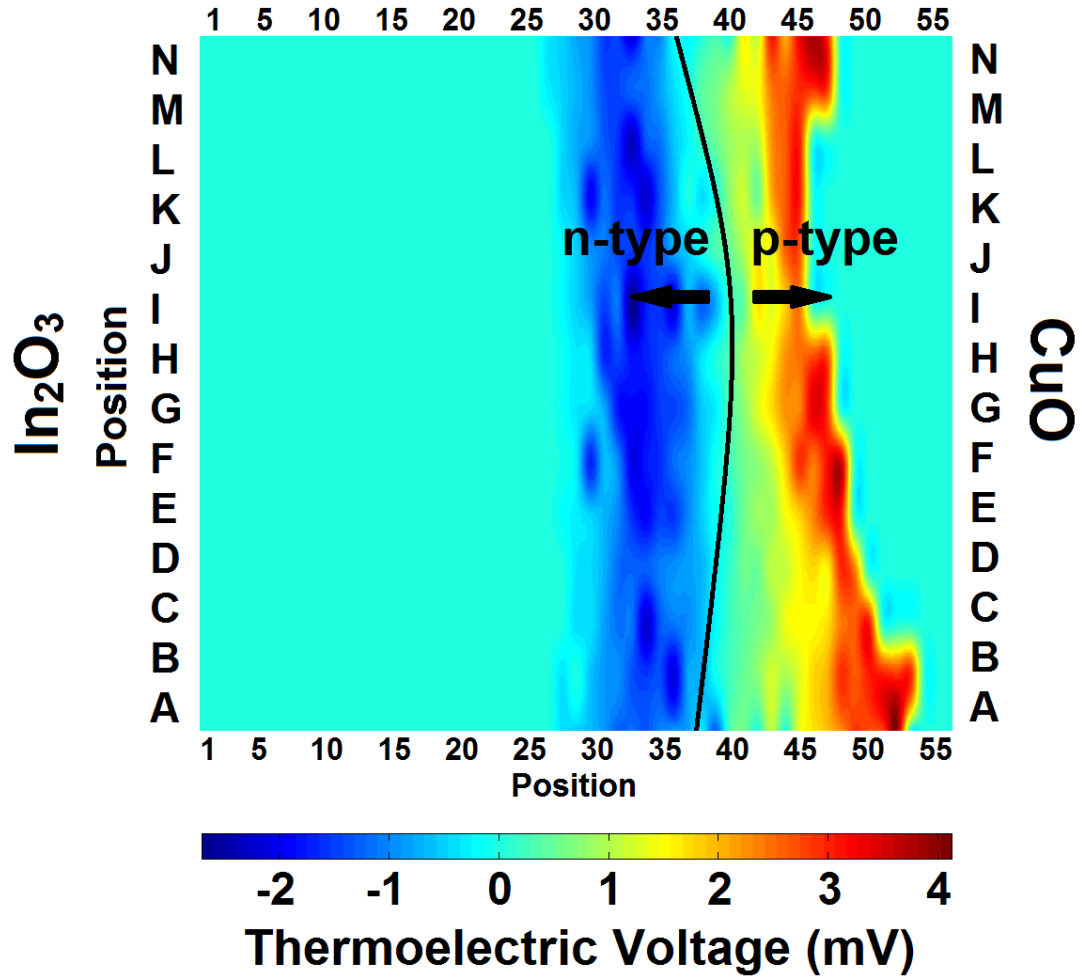

Figure 16. Map of the thermoelectric voltage as a function of composition (at% indium) for nitrogen annealed combinatorial library (a temperature difference of T = 7.7 °C was applied across individual thermocouples).

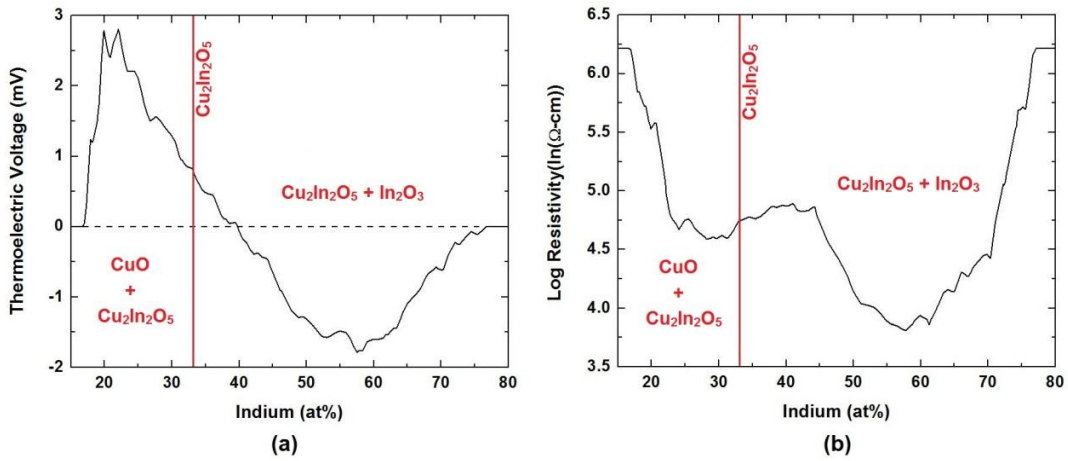

Figure 17. Plots of (a) thermoelectric voltage and (b) electrical resistivity of Cu-In-O films as a function of composition (at% indium) and phase region. Dashed line presented is a guide for the eye to see the p-n transition composition indicated by a change in the sign of the thermoelectric voltage. Red line represents the single phase composition $Cu_2In_2O_5$. The CuO and $Cu_2In_2O_5$ phase region is to the left of the red line and the $Cu_2In_2O_5$ and In_2O_3 phase region is to the right of the red line [10].

25-45 at% indium. However, the thermoelectric response changed by nearly 3 mV over the same range. This phenomenon was likely due to the increased copper oxide content in the films as the indium content was varied from 45 at% to 25 at%. Also apparent in figures 17a and b are horizontal "flat" regions (<15 at% and >75 at% indium) over which reliable thermoelectric measurements could not be obtained because of the high electrical resistivity of the thermo-elements in these composition ranges. Peak thermoelectric voltages for the library thermo-elements exhibiting p-type behavior and n-type behavior occurred between 20-25 at% indium and 50-60 at% indium, respectively. Plots of resistivity as a function of composition (figure 17b) clearly show two minima at 25-30 at% indium and 55-60 at% indium, which are the same compositional ranges as the p-type and n-type materials with the largest thermoelectric responses. It is important to note here that the thermo-elements were not heated in air and thus the use of Cu-In-O thermoelectric materials in oxidizing ambient may be limited.

3.4.2 Crystallography and Phases

XRD patterns of four nitrogen annealed Cu-In-O thermo-elements grown on sapphire substrates are shown in Figure 18. The two copper rich films (35 at% In and 28.5 at% In) exhibited a low intensity CuO {111} peak and no other peaks were observed. As the indium oxide content in the thermo-elements increased (61 at% In, 45.5 at% In), the degree of crystallinity increased as determined by peaks corresponding to $Cu_2In_2O_5$ and In_2O_3 phases. Typically, films in the Cu-In-O system grown at or near room temperature are largely amorphous or have significant amorphous regions [11], which was clearly evident in the copper rich films. However,

the indium oxide rich thermo-elements had well defined crystalline phases, although many of the additional peaks were low in intensity. The presence of CuO, $Cu_2In_2O_5$, and In_2O_3 phases as a function of composition was in close agreement with the phase diagram for the CuO-In_2O_3 system [10]. The investigators established the phase diagram by combining CuO and In_2O_3 in various ratios, sintering them in air, and determining the resulting phase distribution by XRD. The thermo-elements fabricated in the present study were annealed in nitrogen and remained consistent with the phase diagram for this system up to high temperatures in an inert environment such as argon or nitrogen [10].

3.4.3 Microstructure

TEM was used to follow microstructural changes of selected elements from the combinatorial library as a function of heat treatment. The TEM images of various Cu-In-O elements are shown in figures 19 and 20. The electron diffraction patterns of the as-deposited films indicated they were amorphous with little or no fine structure (figure 19a). Annealing of the indium oxide rich films (> 40 at% In) resulted in the formation of small crystallites in an amorphous matrix. As the copper oxide content was systematically increased (< 40 at% In), relatively large, faceted particles were observed (figures 19e & 20a). EDS analysis of those dispersed particles indicated that they have increased oxygen and copper content relative to the surrounding matrix. At lower magnification, figure 20a shows phase separation of highly crystalline, copper oxide particles (dark) against a distinct lighter background matrix. The lighter phase was further magnified to disclose a copper oxide rich phase (light) and indium oxide

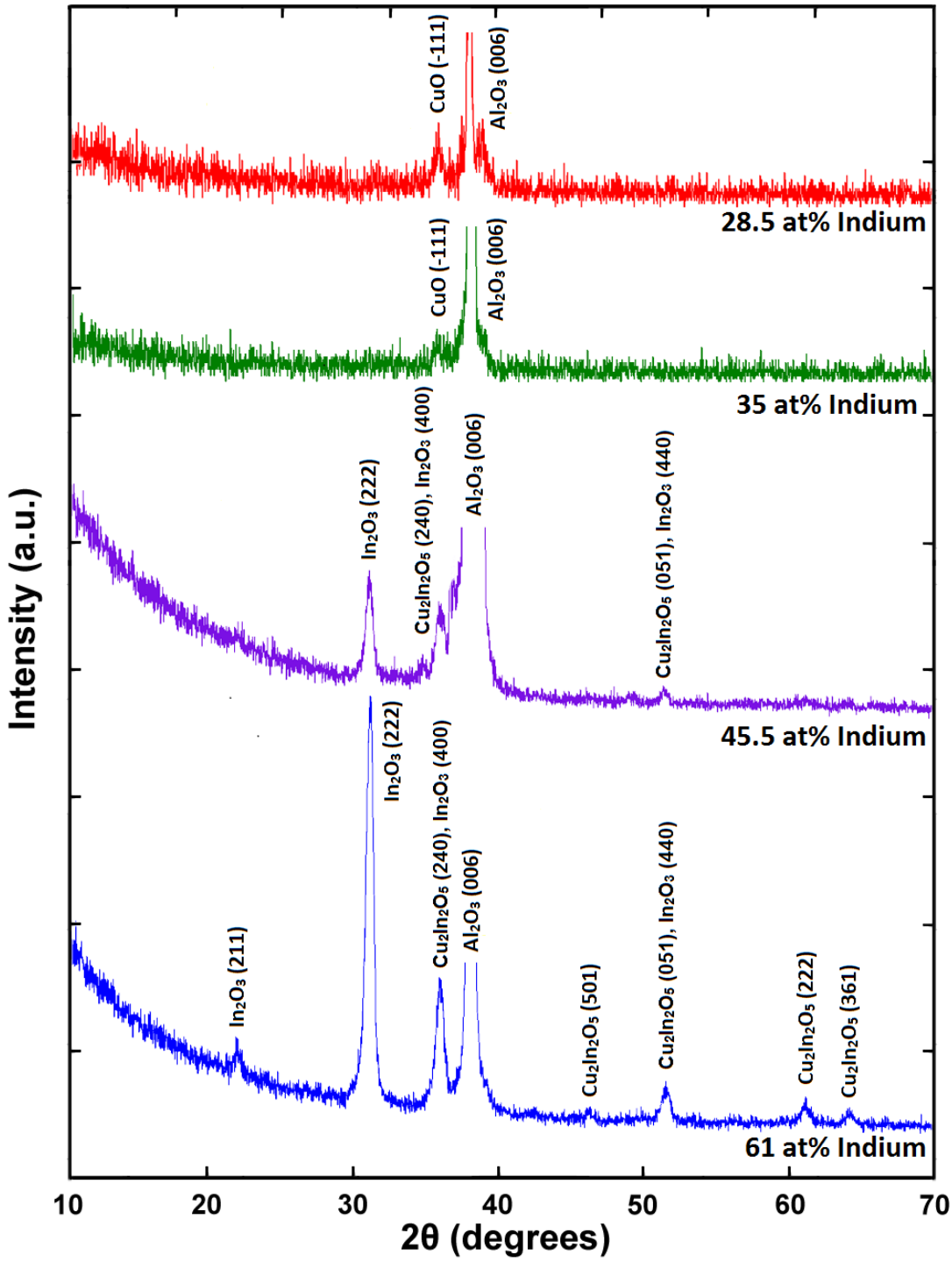

Figure 18. XRD patterns of four Cu-In-O films; three copper oxide rich at 28.5 at% In and 35 at% In and 45.5 at% In and one indium-rich at 61 at% In.

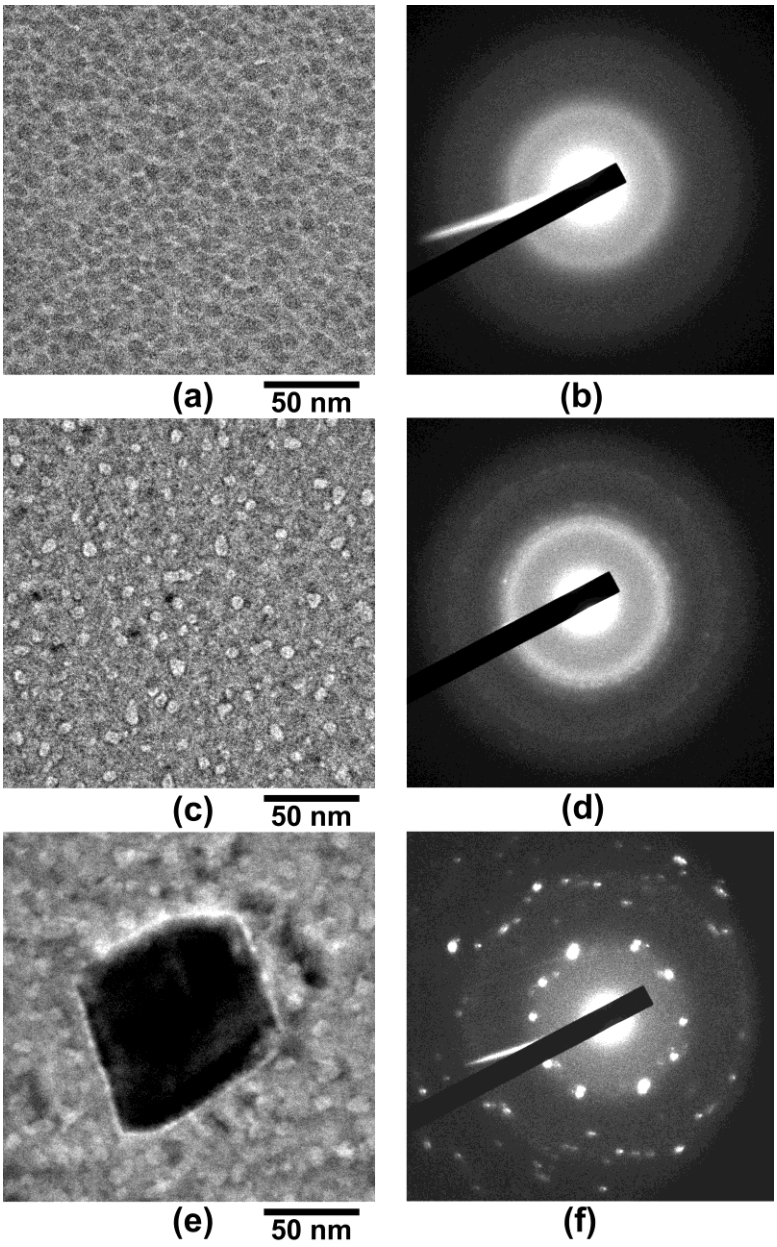

Figure 19. TEM micrographs and electron diffraction patterns for: (a, b) typical as deposited films showing totally amorphous and uniform structure, (c, d) at onset of crystallinity (after 400 °C, 5 h nitrogen anneal), and (e, f) after phase separation of the film into large copper-rich particles.

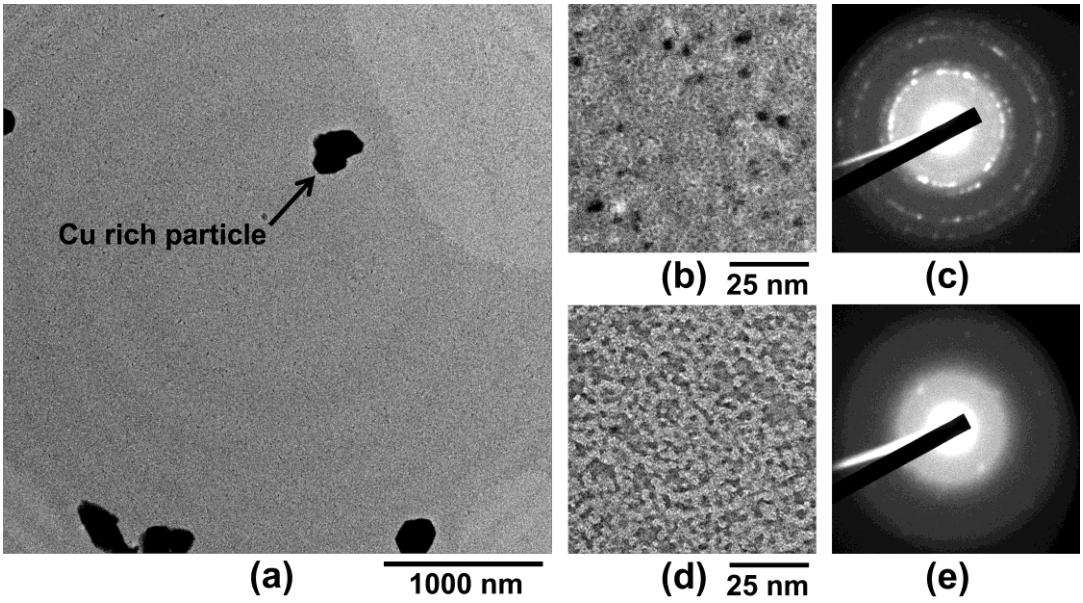

Figure 20. TEM micrographs and electron diffraction patterns showing phase separation in a Cu-In-O film (50 at% In): (a) low magnification image indicating copper-rich precipitates in an amorphous background, (b) high resolution image of copper-rich region with (c) corresponding electron diffraction pattern and (d) high resolution image of (nearly) amorphous background with (e) corresponding electron diffraction pattern.

rich phase (dark) as shown in figures 20b and 20d, respectively with corresponding electron diffraction patterns in figures 20c and 20e. Preferred orientation of the matrix tends to increase as the amount of copper in the thermo-element was increased (figures 19f and 20c). This contrasts with the XRD spectra from above because these same copper rich thermo-elements were amorphous. This was due to the relative size scale at which these measurements were taken. The TEM images corresponded to a much smaller area of the thermo-elements than that examined using XRD. Therefore, variations in the thermo-element crystallinity are prevalent.

3.5 Conclusion

The Cu-In-O thermo-elements with the largest p-type and n-type response are promising candidates for further consideration as thermoelectric materials. Cu-In-O p-n junctions can be fabricated for thermoelectric applications such as thermoelectric generators by sputtering thermo-elements from targets of the same compositions as the best performing p-type and n-type materials to form thermocouples. Additionally, the p-type and n-type thermo-elements will be compatible in terms of thermal expansion during thermal cycling since they are from the same materials system.

List of References

[1]C. G. Granqvist, *Solar Energy Materials and Solar Cells*, **91**, 1529 (2007).

[2]K. Nomura, H. Ohta, A. Takagi, T. Kamiya, M. Hirano, H. Hosono, *Nature*, **432**, 488 (2004).

[3]D. Bérardan, E. Guilmeau, A. Maignan, and B. Raveau, *Journal of Applied Physics*, **104**, 064918 (2008).

[4]E. M. Hopper, Q. Zhu, J-H Song, H. Peng, A. J. Freeman, and T. O. Mason, *Journal of Applied Physics*, **109**, 013713 (2011).

[5]D. Bérardan, E. Guilmeau, A. Maignan, and B. Raveau, *Solid State Communications*, **146**, 97-101 (2008).

[6]H. Kaga, R. Asahi, and T. Tani, *Japanese Journal of Applied Physics*, **43** (6a), 3540-3543 (2004).

[7]M. Amani, I. M. Tougas, O. J. Gregory, and G. C. Fralick, *Journal of Electronic Materials*, **42** (1), 114-120 (2013).

[8]M. Yin, C-K. Wu, Y. Lou, C. Burda, J. T. Koberstein, Y. Zhu, and S. O'Brien, *Journal of the American Chemical Society*, **127** (26), 9506-9511 (2005).

[9]J-C Lee, Y-W Heo J-H Lee, and J-J Kim, *Thin Solid Films*, **518**, 1234 (2009).

[10]M. Bosacka, E. Filipek, P. Šulcova, Ž. Dohnalová, and A. Paczesna, *Journal of Thermal Analysis and Calorimetry*, **109**, 605-610 (2012).

[11]A. V. Chadwick, A. N. Blacklocks, A. Rougier, and C. Yaicle, *Journal of Physics: Conference Series*, **249**, 012045 (2010).

[12]H. Kawazoe, M. Yasukawa, H. Hyodo, M. Kurita, H. Yanagi, and H. Hosono, *Nature*, **389**, 939 (1997).

[13]L. Liu, K. Bai, H. Gong, and P. Wu, *Chemistry of Materials*, **17**, 5529-5537 (2005).

[14]H. Yanagi, T. Hase, S. Ibuki, K. Udea, and H. Hosono, *Applied Physics Letters,* **78**, 1583 (2001).

[15]M. Shimode, M. Sasaki, and K. Mukaida, *Journal of Solid State Chemistry*, **151**, 16 (2000).

CHAPTER 4

THIN FILM PLATINUM-PALLADIUM THERMOCOUPLES FOR GAS TURBINE ENGINE APPLICATIONS

4.1 Abstract

Thin film platinum:palladium thermocouples were fabricated on alumina and mullite surfaces using radio frequency sputtering and characterized after high temperature exposure to oxidizing environments. The thermoelectric output, hysteresis, and drift of these sensors were measured at temperatures up to 1100 °C. Auger electron spectroscopy was used to follow the extent of oxidation in each thermocouple leg and interdiffusion at the metallurgical junction. Minimal oxidation of the platinum and palladium thermoelements was observed after high temperature exposure, but considerable dewetting and faceting of the films was observed in scanning electron microscopy. An Arrhenius temperature dependence on the drift rate was observed and later attributed to microstructural changes during thermal cycling. The thin film thermocouples, however, did exhibit excellent stability at 1000 °C with drift rates comparable to commercial type-K wire thermocouples. Based on these results, thin film thermocouples based on platinum:palladium have considerable potential for use in the hot sections of gas turbine engines.

Tougas and Gregory, *Thin Solid Films, in press (2013).*

4.2 Introduction

Gas turbine engine components based on advanced ceramics such as ceramic matrix composites have superior thermomechanical properties at temperatures above 1000 °C when compared to conventional superalloys [1]. Additionally, ceramic thermal barrier coatings have enabled gas turbine engine blades comprised of superalloys to operate at temperatures as high as 1500 °C [2], which translates into both improved fuel efficiency and reduced NO_x emissions. Due to the severe temperature gradients that can exist in these advanced materials, there is a need to integrate sensors into these components to monitor their thermomechanical behavior. Thin film sensors can be directly deposited onto both stationary and rotating engine components for health monitoring as well as to verify existing models [1-3].

Thin film thermocouples offer several advantages over conventional wire thermocouples or thermal spray instrumentation used in gas turbine engine applications. Thin film sensors do not adversely affect gas flow patterns through the engine since their thicknesses are well below the boundary layer thickness formed on rotating surfaces [3, 4]. Thin film sensors also have negligible mass and therefore have minimal effect on the vibrational modes of rotating components [5]. They are more accurate and have faster response times than conventional wire sensors (< 1 μs) due to their lower thermal mass. Additionally, thin films are not affected by the g forces acting on the blades which are rotating at high velocities [3, 6]. Furthermore, the films can be directly deposited onto the surface of engine components without the need for adhesives, permitting more accurate surface temperature measurements than wire based sensors [3].

Wire thermocouples have been employed in engine applications for more than 30 years, however, the presence of oxygen can cause instability and drift at temperature in metallic thin film thermocouples due to the significantly reduced diffusional distances in these devices. For example, conventional type-S thin film (platinum:90 % platinum-10 % rhodium) thermocouples can suffer from selective de-alloying of rhodium in the film due to the formation of rhodium oxides at temperatures between 600-800 °C [7]. This results in a progressive, time dependent degradation or drift in the thermoelectric output by as much as 5 °C/h as the platinum-rhodium thermocouple legs undergo microstructural and compositional changes due to this selective oxidation [3]. This effect can be mitigated by applying alumina overcoats to protect the thermocouple elements from oxidation [3, 7]. Therefore, there is a need for more stable thermocouple materials that do not experience detrimental microstructural changes and selective oxidation issues at high temperature without resorting to protective overcoats.

Platinum-rhodium alloys are currently being employed as complementary thermoelements for wire-based thermocouples and thin film-based thermocouples. However, noble metals such as gold, palladium, and platinum do not suffer from selective oxidation processes at elevated temperatures since they are not alloys. Unfortunately, the use of gold for high temperature thermocouple applications above 1000 °C is limited due to its low melting point (1064 °C) and dewetting of the metal on oxide substrates at temperatures of 900 °C [8]. Wire thermocouples based on platinum and palladium have been investigated to some extent [9-13], however, investigations of thin film platinum:palladium thermocouples have been somewhat

limited. Kreider et al. has examined the use of thin film platinum:palladium thermocouples on oxidized silicon wafers for radiometric temperature measurements up to 1050 °C [14, 15]. However, these thermocouples could only measure temperatures up to 850 °C and required the use of a titanium bond coat between the silicon wafer and thermocouple elements due to dewetting issues [14, 15]. The use of thin film platinum:palladium thermocouples for higher temperature applications has not been previously investigated.

In this study, platinum:palladium thin film thermocouples were deposited onto ceramic substrates, including alumina and mullite, using r.f. sputtering. The thermoelectric output and drift were measured at temperatures up to 1100 °C and these thin film thermocouples exhibited remarkable stability at high temperature in an oxidizing environment. Auger electron spectroscopy (AES) was used to characterize the chemical composition of the metallurgical junctions as a function of depth and to monitor the extent of oxidation of the junction. The microstructure of the thermocouple legs and metallurgical junctions were examined using scanning electron microscopy (SEM).

4.3 Experimental details

Both alumina and mullite (CoorsTek, Inc.) were employed as the substrates for all thin film platinum:palladium thermocouples. The substrates (190 mm x 25 mm x 2 mm) were cleaned with acetone, methanol, and deionized water. A dry film negative photoresist (DuPont^{TM} MX 5050^{TM}) was applied to the surface of the substrates and was soft-baked prior to patterning thin film thermocouples. After application of the

photoresist, the thin film thermocouple patterns were transferred to the resist using an Optical Associates, Inc. aligner (350 nm wavelength ultraviolet light) to expose the resist. The photoresist coated substrates were developed to reveal the desired pattern and placed inside a Materials Research Corporation model 8667 sputtering system to deposit the metal thermocouple legs. Platinum and palladium films were deposited in pure argon. A background pressure of 2.7×10^{-4} Pa was achieved in the sputtering chamber prior to sputtering and the stage (work piece) was maintained at temperatures below 100 °C using water-cooling. Table 4 lists the sputtering parameters employed to deposit the platinum and palladium films. Deposition resulted in 1.5 μm of platinum and 2 μm of palladium.

All thin films were annealed in nitrogen for 5 h at 500 °C to remove point defects, including trapped argon, and densify the films. The thermoelectric output was measured as a function of time and temperature by placing the metallurgical junction (hot junction) in the hot zone of a tube furnace and attaching the cold junction to an aluminum chill block outside the furnace. In this way, a temperature difference was applied along the length of the beam and the cold junction was maintained at or below 100 °C using chilled water. The thermocouples were thermally cycled in air to 900 °C at 4 °C/min for several cycles to determine the thermoelectric voltage and the drift rate was determined at 800 °C, 900 °C, 1000 °C, and 1100 °C over a 10 h period at each temperature. The temperature difference was continuously monitored using type-K (cold junction) and type-S (hot junction) wire thermocouples and copper extension wires were attached to the bond pads of the platinum:palladium thermocouples using a silver paste to acquire the voltage signals. All copper wires and wire thermocouples

Sputtering Parameters	Target Diameter (cm)	Target Power (W)	Power Density (W/cm^2)	Sputtering Gas Pressure (Pa)	Deposition Rate (μm/h)	Film Thickness (μm)
Platinum	10.16	200	3.88	1.20 Ar	0.6	1.5
Palladium	12.70	200	2.49	1.20 Ar	1.0	2.0

Table 4. Sputtering parameters used for the deposition of platinum and palladium.

were connected to an IOTech Personal Daq 54 USB data acquisition system with *PDaq View Plus*© software recording the temperature and voltage signals. AES depth profiles were used to determine the chemical composition of the metallurgical junction and identify oxidation products formed on the platinum and palladium thermocouple legs. AES was performed using a Perkin Elmer 5500 Multi-Technique Surface Analyzer. A background pressure of $6.0x10^{-7}$ Pa was established and a 1x1 mm area on the surface of each thermocouple sample was sputter cleaned for 10 seconds prior to acquiring each depth profile. SEM was performed on the same films to analyze the microstructure after thermal cycling using a JEOL JSM-5900LV SEM and a 20 kV accelerating voltage.

4.4 Results and Discussion

4.4.1 Thermoelectric measurements

The thermoelectric response of several platinum:palladium thin film thermocouples are shown in Fig. 21a and Fig. 21b. A peak temperature of 900 °C was employed at the hot junction during thermal cycling and a temperature difference as large as 750 °C was established along the length of the ceramic substrates. The maximum thermoelectric voltage of thin film thermocouples subjected to a temperature difference of 750 °C was 9.00 mV on alumina substrates and 9.52 mV on mullite substrates. This thermoelectric response was comparable to a conventional type-S wire thermocouple, which typically has a thermoelectric response of 8.45 mV, when a similar temperature difference is applied [16]. Remarkable stability was observed for the thin film platinum:palladium thermocouples when tested over several

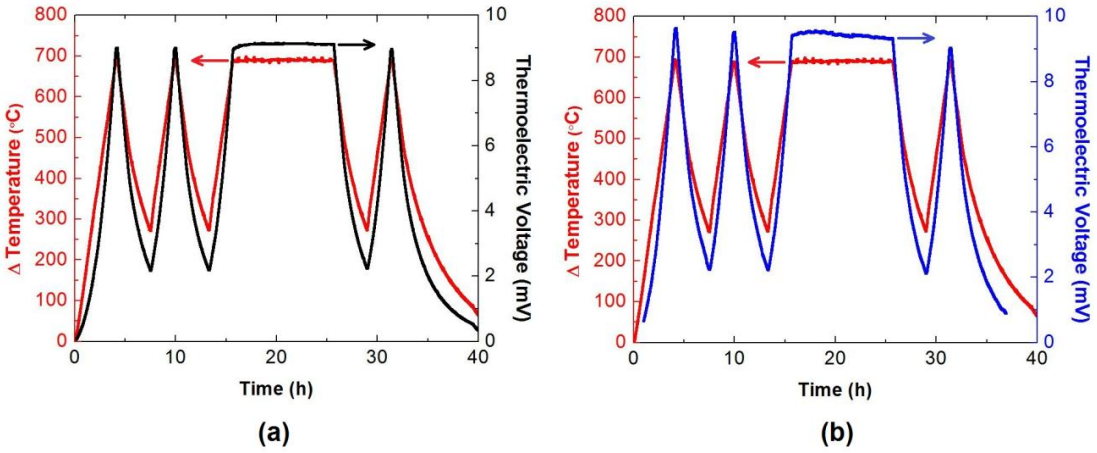

Figure 21. Thermoelectric output of two different platinum:palladium thermocouples on alumina (a) and mullite (b). A peak hot junction temperature of 900 °C was used in each case.

thermal cycles. However, the peak thermoelectric voltage at 900 °C for the thin film thermocouples diminished slightly after each temperature ramp, which most likely results from microstructural changes such as grain growth, pore growth, and dewetting of the metallic films. Hysteresis upon heating and cooling to 900 °C is shown in Fig. 22. Here, the thin film thermocouples on mullite exhibited greater hysteresis than those formed on alumina. However, the hysteresis was comparable to that of previously studied ceramic thin film thermocouples deposited on alumina [2]. Furthermore, ceramic films have inherently greater stability in air because they have all the oxygen that they can take in their structures.

The Seebeck coefficient and drift rates of the thin film thermocouples were determined as a function of hot junction temperature and time, respectively. The Seebeck coefficient defined in this study is given by Eq. 1

$$S = \frac{-\Delta V}{\Delta T} = -\left(\frac{\Delta V_a - \Delta V_b}{T_h - T_c}\right) \tag{1}$$

where S is the Seebeck coefficient given in μV/°C, ΔV is the voltage potential difference between the two thermocouple materials ($\Delta V_a - \Delta V_b$), and ΔT is the temperature difference between the hot junction (T_h) and the cold junction (T_c). Eq. 2 gives the temperature dependence of the Seebeck coefficient for metal thermocouples

$$S(N_D) = -\left(\frac{\pi}{3N_D}\right)^{2/3}\left(\frac{8k^2 m^* T}{3e\hbar^2}\right)\left(A + \frac{3}{2}\right) \tag{2}$$

where N_D is the carrier concentration, k is the Boltzmann constant, m^* is the effective electron mass, T is the absolute temperature, e is the electron charge, and A is a transport constant [2]. There is no appreciable change in the carrier concentration of these highly conductive platinum and palladium films over the temperature range of

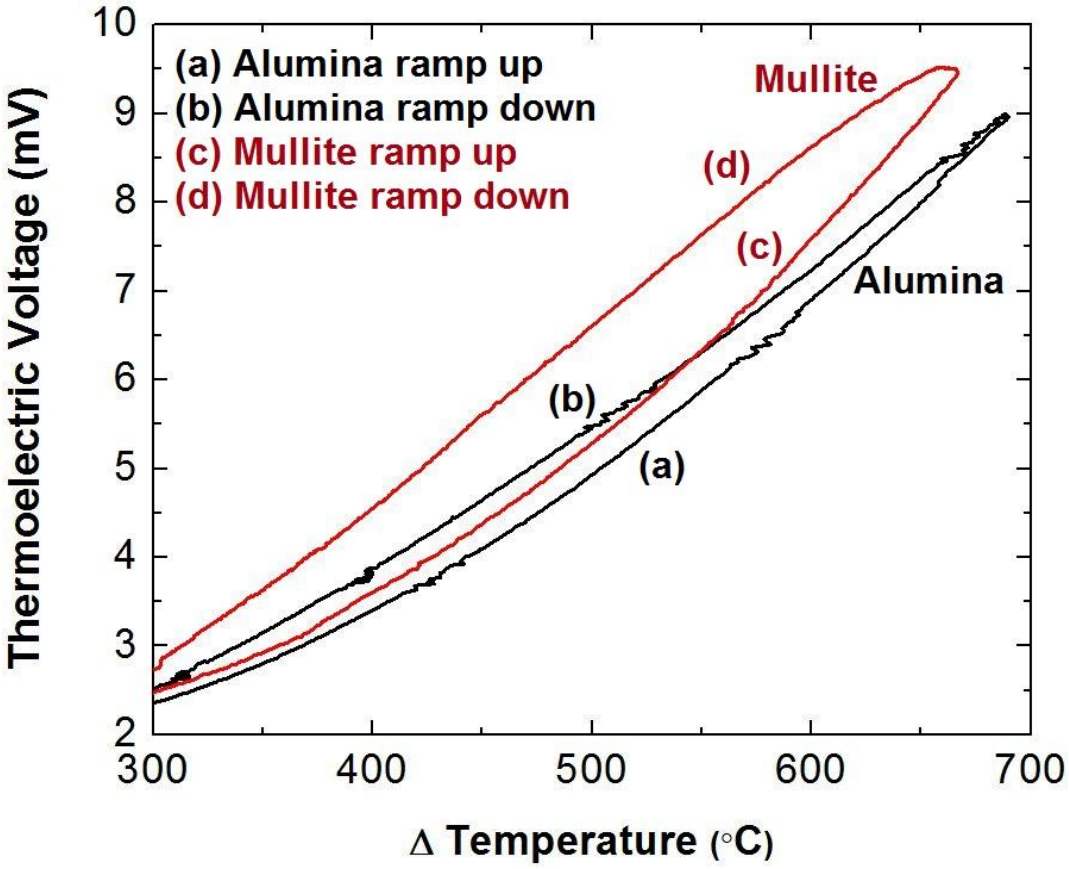

Figure 22. Hysteresis upon heating/cooling platinum:palladium thermocouples on alumina and mullite. Corresponds to second cycle of thermoelectric data in Figure 21a and Fig. 21b.

interest, and it was observed that the Seebeck coefficient increased in a linear fashion over most of the temperature range investigated, as shown in Fig. 23. Therefore, the Seebeck coefficient, which was expected to be a linear function of temperature, was confirmed in this study.

Thermocouple drift was defined according to Eq. 3 below

$$DR(T) = \frac{\Delta V(T)}{V(T)_{ref}} \cdot \frac{T}{\Delta t} \tag{3}$$

where $DR(T)$ is the drift rate given in °C/h, $\Delta V(T)$ is the change in voltage at constant temperature, $V(T)_{ref}$ is the initial voltage, T is the temperature, and Δt is the elapsed time at temperature. Table 5 shows the drift rate of thin film platinum:palladium thermocouples on alumina and mullite surfaces at different temperatures. Table 6 gives equation parameters for the relationship between temperature difference and voltage for the platinum:palladium thermocouples on alumina and mullite surfaces. The drift rates of these thin film thermocouples were less than 1 °C/h in magnitude at temperatures up to 1000 °C. Microstructural changes in the films during thermal cycling may have been responsible for drift since the drift rate had an apparent Arrhenius temperature dependence. Fig. 24 shows the Arrhenius temperature dependence on drift rate for thin film platinum:palladium thermocouples deposited on alumina. This Arrhenius temperature dependence was modeled according to Eq. 4 below:

$$DR(T) = A \cdot exp\left(-\frac{E_a}{RT}\right) \tag{4}$$

where A is a constant, E_a is the activation energy, R is the gas constant (8.314 J/mol·K), and T is the absolute temperature. The activation energy associated with the

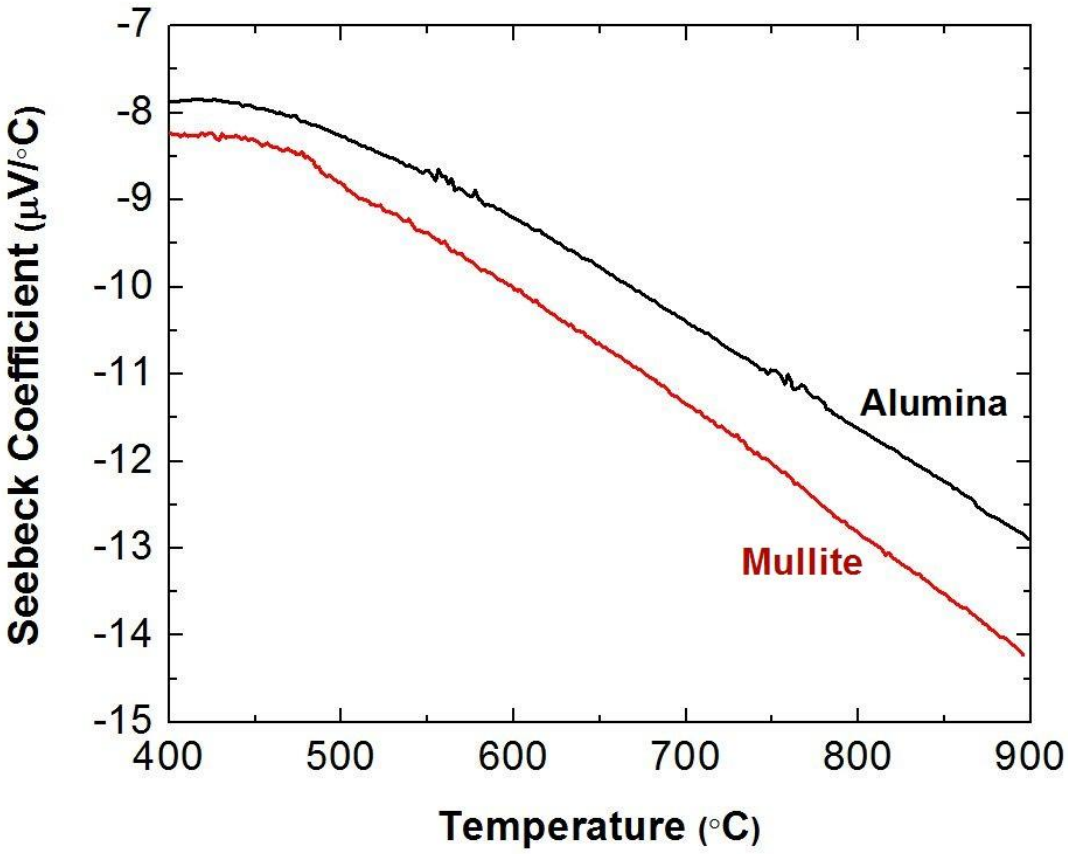

Figure 23. Seebeck coefficient of platinum:palladium thermocouples on alumina and mullite as a function of temperature and substrate.

Drift Rate (°C/h)	800 °C	900 °C	1000 °C	1100 °C
Alumina	0.18	-0.06	-0.76	-2.06
Mullite	-1.46	-0.83	-	-

Table 5. Drift rates of platinum:palladium thermocouples on alumina and mullite at various temperatures.

	$V(\Delta T) = A(\Delta T)^3 + B(\Delta T)^2 + C(\Delta T)$		
	A	B	C
Alumina	2E-05	5E-04	0.8444
Mullite	1E-05	4.9E-03	-0.0271

Table 6. Equation parameters for the relationship of temperature difference to voltage for platinum:palladium thermocouples on alumina and mullite surfaces.

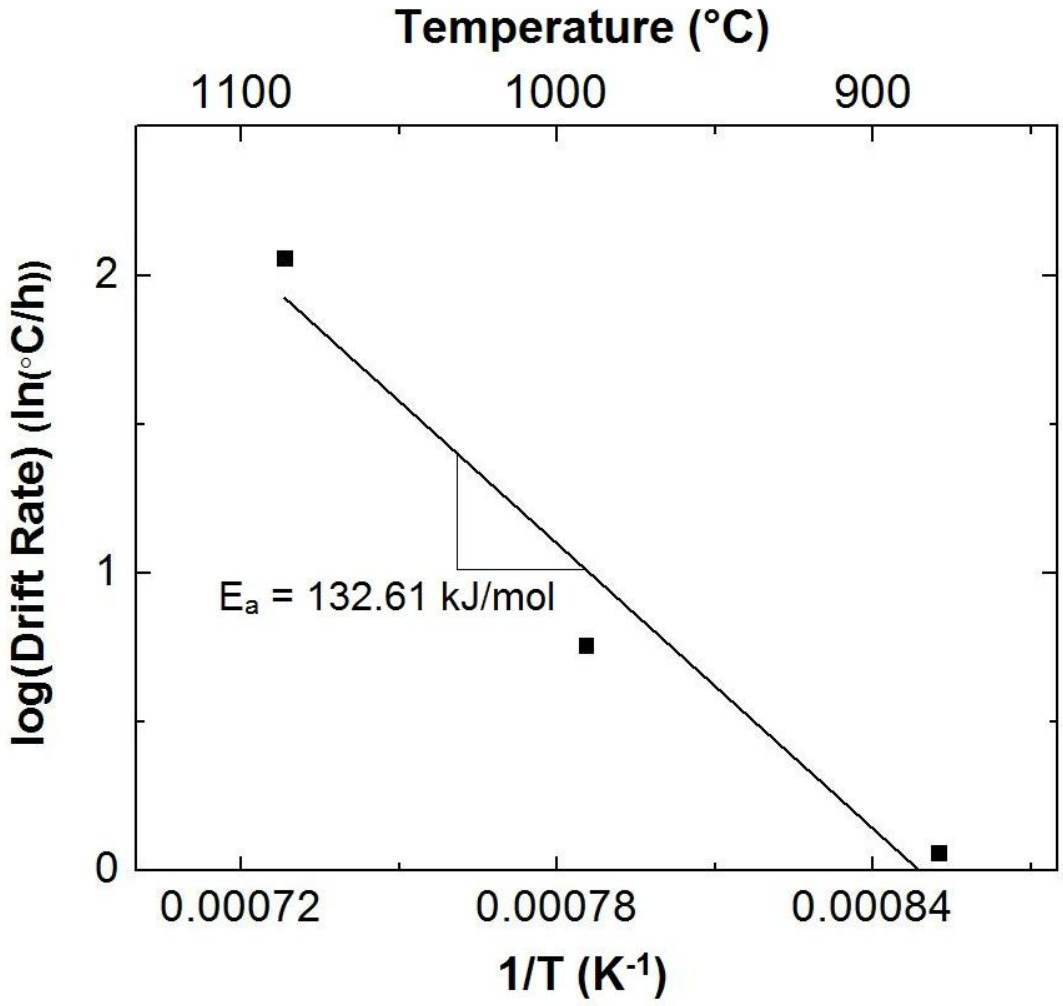

Figure 24. Drift rates of platinum:palladium thermocouples as a function of temperature. Note the Arrhenius temperature dependance of the drift rates.

drift rate of the platinum:palladium thin film thermocouples was 132.61 kJ/mol, as given by the slope of the log of drift rate versus 1/T. This activation energy falls between the activation energies for surface diffusion and volumetric diffusion of platinum and palladium, which suggests that a combination of surface driven forces and bulk microstructural changes were responsible for the observed drift [17]. Processes such as the constrained grain growth and dewetting, which reduce the surface free energy of the films, are the most likely the causes of drift. Nonetheless, the drift rates of these platinum:palladium thermocouples were comparable to wire type-K thermocouples operating at temperatures up to 1100 °C, confirming that they have remarkable stability relative to current commercially available instrumentation.

4.4.2 AES depth profiling and SEM imaging

The chemical composition of the thin film thermocouples, at the metallurgical junctions, was determined as a function of depth using AES. Oxide formation on platinum was limited to thicknesses less than 1 nm, regardless of the substrate used. Oxygen was present at no more than 5 atomic percent throughout the cross-section and was likely detected from the alumina or mullite substrates where dewetting of the metallic films had occurred. Oxygen solubility in platinum and palladium is very low (on the order of 0.035 atomic percent in palladium at 4.0×10^4 Pa oxygen partial pressure and 850-900 °C) [18]. Platinum does not readily form an oxide at temperatures above 500 °C but instead experiences material loss through the evaporation of the metal or one of its volatile oxides, such as PtO_2 [19, 20]. The loss of platinum due to evaporation is proportional to the oxygen partial pressure in the

ambient, and is appreciably higher at atmospheric pressure between 1000 °C and 1100 °C, where PtO_2 has a partial vapor pressure of 0.05 Pa [19]. Decomposition of the volatile oxides at high temperature can result in the redeposition of the metal onto the original surface, so the overall material loss is minimal compared to other noble metals [19]. Therefore, any oxides that were present on the surface of the platinum legs likely formed during cooling from elevated temperatures.

Oxide formation on palladium when deposited on alumina was limited to a thickness of less than 1 nm, which was comparable to that of platinum films formed on the same surface. Again, oxygen was still detected at greater film depths but was likely due to the exposed substrate in areas where the metal film had dewetted. Oxygen was detected at approximately 30 atomic percent to a depth of more than 25 nm for palladium deposited on mullite. However, the formation of condensed oxide phases on the palladium is not likely; while material loss from evaporation of the metal or of its volatile oxide, PdO, is much more likely [19]. At temperatures greater than 850 °C, surface oxides on palladium typically decompose. The vapor pressure of palladium metal at temperatures above 1000 °C exceeds that of PdO, especially at atmospheric pressure, so material loss due to palladium metal evaporation likely dominates the material loss mechanism [19, 20]. Therefore, it is likely that the high atomic percentage of oxygen detected in the films is derived from the exposed mullite surface in the vicinity of the dewetted palladium films. This dewetting phenomenon was much more prevalent in the palladium films than platinum, as given by the atomic percent oxygen detected for both thin films.

Considerable interdiffusion of platinum and palladium at the metallurgical junctions of the thin film thermocouples was verified by AES depth profiling. Since a complete solid solution of platinum and palladium will be formed at the junction, solid solutions containing approximately 90/10 atomic percent platinum/palladium on alumina and 78/22 atomic percent platinum/palladium on mullite were not surprising. The platinum-palladium phase diagram provided further evidence of solid solution formation in both metallurgical junctions [21]. Oxygen was detected at depths up to 15 nm at both metallurgical junctions; however, the detection of oxygen was most likely from exposed substrate surfaces since it is not likely a metastable oxide film would form at these depths in either platinum or palladium [19]. A larger atomic percentage of oxygen in the metallurgical junction was detected on mullite because it experienced a greater amount of dewetting after thermal cycling than the same junction formed on alumina.

Dewetting in conjunction with faceting of both the platinum and palladium films were observed in SEM, and these microstructural changes were apparent in the thin film thermocouples deposited on both alumina and mullite. In all cases, dewetting resulted in recrystallization and pore growth where the pore edges were faceted, particularly at grain boundaries. Fig. 25 shows the microstructure of platinum and palladium films on alumina and mullite. When deposited on alumina, the palladium films contained larger pore sizes along with larger grains and more faceting, than observed in the platinum films due to differences in the melting temperature of the two metals. Furthermore, the surface recession rate of palladium is four orders of magnitude higher than platinum due to surface energy considerations [19].

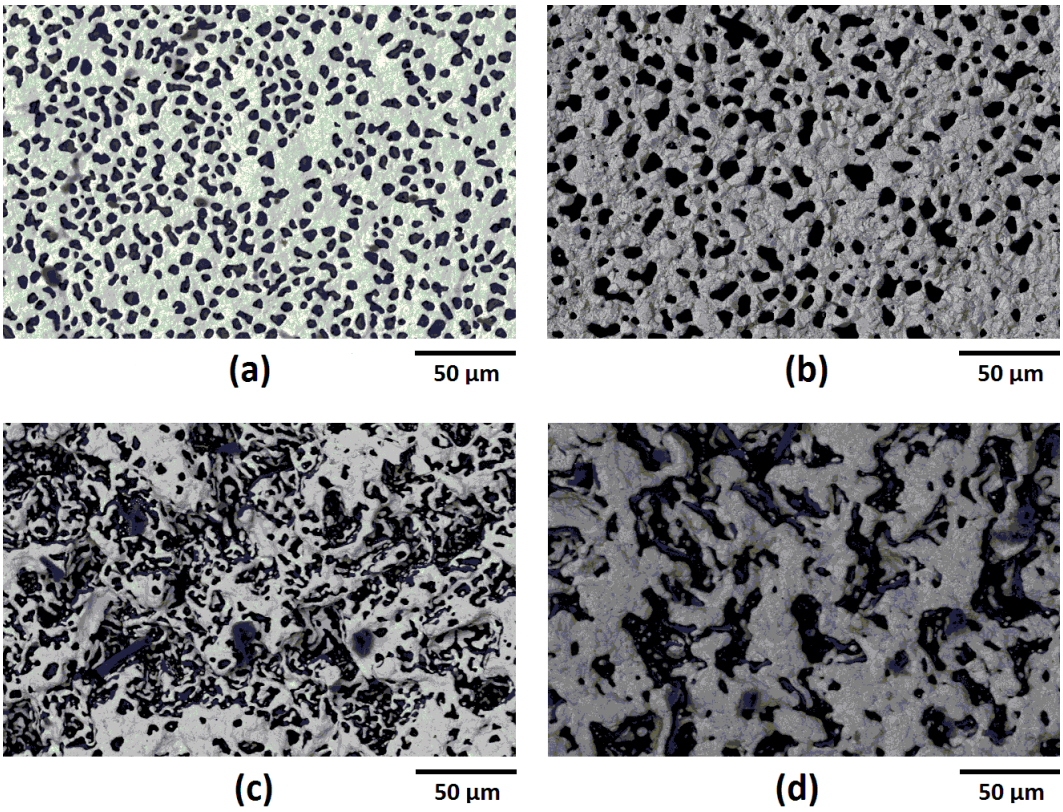

Figure 25. SEM micrographs using backscatter electron imaging (BSEI) of various thin film thermocouple legs after high temperature cycling: platinum on alumina (a); palladium on alumina (b); platinum on mullite (c); and palladium on mullite (d). Each film exhibited dewetting with distinctly different microstructures due to long term high temperature exposure.

When deposited on mullite, the platinum resembled a contiguous network of high aspect ratio crystals and faceted islands with discrete pores. Palladium films deposited on mullite appear to have similar dewetting characteristics relative to the palladium film formed on alumina. Due to differences in surface roughness, the topography of the palladium film appears different on mullite because it generally contains larger pores and randomly dispersed smaller islands, which were not observed in the films formed on alumina. The differences in the dewetting of these films results from dissimilar surface energy and surface roughness of the substrates, where the rougher surfaces tend to induce more residual stress on films, increasing their surface free energy. Therefore, there is a greater driving force for dewetting of platinum and palladium on mullite due to its relatively rougher surface. This is primarily responsible for the different microstructures observed on alumina. All microstructures here appeared to be similar to those formed via a vapor phase transport mechanism, in which continuous and fully faceted networks of metal were formed throughout the film due to the dewetting process [3]. Higher magnification revealed faceted striations in the thermocouple legs, which are also suggestive of the vapor phase transport. Various images of striations in the films are shown in Fig. 26a and Fig. 26b.

The microstructure of the metallurgical junctions showed no evidence of phase separation since a complete solid solution was formed between platinum and palladium after thermal cycling. The formation of faceted pores was evident in the dewetted films; however, the extent to which this occurred in relation to platinum and palladium was minimal. This was due to the increased thickness of the overlapping platinum and palladium films at the junction relative to the individual legs. If more

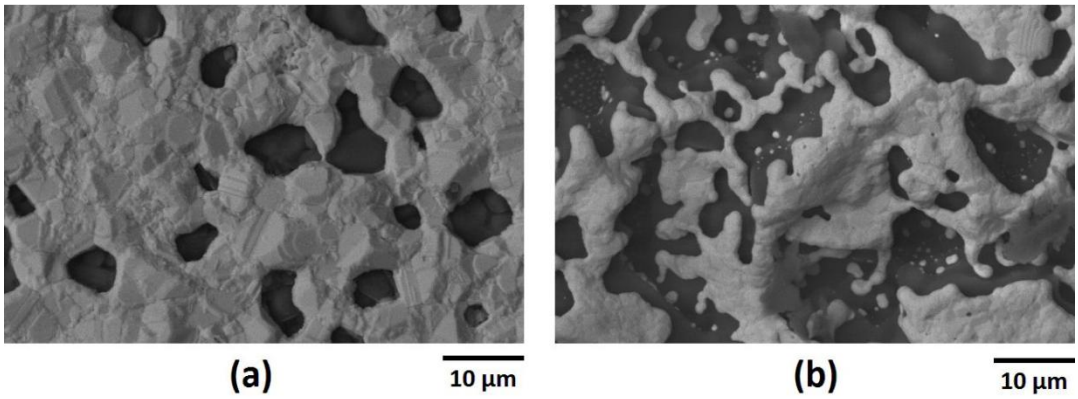

Figure 26. SEM micrographs (BSEI) of the faceted striations in the thermocouple legs after high temperature cycling: palladium on alumina (a); platinum on mullite (b).

material is initially present, as in the case of the thermocouple junctions, the dewetting process has the same microstructural effect. Similar to the platinum and palladium films, faceted striations were observed at the metallurgical junction on both surfaces. Delamination of the film was also observed at the metallurgical junction/palladium interface where the junction had receded from the palladium film and was likely driven by dewetting of the palladium film during thermal cycling. Delamination and dewetting of these films would ultimately lead to device failure where, in the limit, the platinum and palladium films would debond completely, most likely at the junction/thermocouple leg interface.

4.5 Conclusion

Platinum:palladium thermocouples were developed to replace conventional thin film thermocouples based on platinum-rhodium alloys. These alloys suffer from high drift rates due to instability and degradation as a result of compositional changes and selective oxidation processes during thermal cycling. The platinum:palladium thin film thermocouples did not show the detrimental effects of selective oxidation and its adverse effect on the chemical stability of the metallurgical junction. Therefore, the drift rates observed for these thermocouples were comparable to conventional type-K wire thermocouples during thermal cycling. Thicker (thin film) thermocouples would prolong the stability of these sensors by inhibiting dewetting and unfavorable microstructural changes in the films during thermal cycling. The thermoelectric performance of these thermocouples at high temperature makes them promising candidates for implementation in the harsh environments of gas turbine engines, and

given their stability, long term sensing at temperatures in excess of 1100 °C will be possible.

List of References

[1] J. D. Wrbanek, G. C. Fralick, and D. Zhu, Thin Solid Films 520 (2012) 5801.

[2] O. J. Gregory, M. Amani, I. M. Tougas, and A. J. Drehman, J. Am. Ceram. Soc. 95 (2012) 705.

[3] G. E. Aniolek and O. J. Gregory, Surf. Coat. Tech. 68-69 (1994) 70.

[4] J. F. Lei and H. A. Will, Sens. Actuators, A 65 (1998) 187.

[5] L. C. Martin and R. Holanda, NASA TM-106714, (1994).

[6] H. Choi and X. Li, Sens. Actuators, A 136 (2007) 118.

[7] K. G. Kreider, J. Vac. Sci. Technol., A 11 (1993) 1401.

[8] D. Wang and P. Schaaf, J. Mater. Sci.: Mater. Electron. 22 (2011) 1067.

[9] K. D. Hill, Metrologia 39 (2002) 51.

[10] M. G. Ahmed and K. Ali, J. Metrology Soc. India 23 (2008) 225.

[11] G. W. Burns, D. C. Ripple, and M. Battuello, Metrologia 35 (1998) 761.

[12] Y. A. Abdelaziz, F. M. Megahed, and M. M. Halawa, Measurement 35 (2004) 413.

[13] N. P. Moiseeva, Meas. Tech. 47 (2004) 915.

[14] K. G. Kreider and G. Gillen, Thin Solid Films, 376 (2000) 32.

[15] K. G. Kreider and F. DiMeo, Sens. Actuators, A 69 (1998) 46.

[16] Revised Thermocouple Reference Tables: Type S, Omega Engineering, Stamford, CT. [http://www.omega.com/temperature/Z/pdf/z208-209.pdf]

[17] I. Beszeda, E. G. Gontier-Moya, and D. L. Beke, Surf. Sci., 547 (2003) 229.

[18] J. Gegner, G. Hörz, and R. Kirchheim, J. Mater. Sci., 44 (2009) 2198.

[19] H. Jehn, J. Less-Common Met., 100 (1984) 321.

[20] J. C. Chaston, Platinum Metals. Rev., 19 (1975) 135.

[21] S. R. Bharadwaj, A. S. Kerkar, S. N. Tripathi, and S. R. Dharwadkar, J. Less-Common Met., 169 (1991) 167.

CHAPTER 5

FUTURE WORK

5.1 Thin Film Thermocouples

Gas turbine engines consume immense amounts of energy from combusting fuels in order to produce thrust or energy for the generation of electricity. In order to meet increasing energy regulations, engine companies are putting tireless effort into improving the efficiency of gas turbine engines. One fundamental way in which this is being progressively achieved is through increasing the operating temperature of the hot section inside the engine. With higher temperatures comes increased efficiency which is defined simply by Carnot's theorem given as $\eta = 1 - T_C/T_H$ where T_C is the cold reservoir temperature and T_H is the hot reservoir temperature. Therefore, by increasing the hot section temperature relative to the surroundings, the thermodynamic efficiency of these engines will increase.

As a result, gas turbine engine manufacturers are met with new challenges to design materials and sensors which can handle the increasingly harsh high temperature environment inside the engine hot section of these more efficient engines. Conventional superalloy materials cannot withstand the 1500°C or higher hot section temperatures in these new engines, therefore ceramic matrix composite (CMC) materials are being developed and employed in these next generation engines. These materials can withstand the increased operating temperatures with superior thermomechanical properties and lower mass relative to superalloy materials. Silicon

carbide based CMCs are currently being developed for implementation inside engine hot sections as turbine blades and components of the combustion chamber. Other issues also arise with the implementation of these CMC materials, such as the need for alternative thermal barrier coatings (TBC) on the surface of parts. These TBCs must have similar thermal expansion coefficients to the CMC so that they exhibit great adhesion during thermal cycling. Additionally, there is a need to develop new sensors or modify existing sensors so they are with the TBCs implemented on CMC components, and they must be able to withstand the increased hot section temperatures. Research has already begun to instrument CMCs for gas turbine engine applications.[1] The CMC, TBC, and thermocouples must be integrated in the following way:

- The TBC must planarize the CMC material prior to the implementation of a thermocouple while also providing environmental protection.
- The TBC must form a dielectric barrier between the CMC material and the thermocouple.
- The thermocouple materials chosen should have similar thermal expansion coefficients to the TBC material and be able to withstand the extreme temperatures over long periods and many cycles.

Based on the work in this thesis, the most promising thermocouple materials for the instrumentation of CMC materials are In_2O_3-ITO and Pt-Pd based. By sticking to the above guidelines carefully and designing experiments accordingly, the implementation of sensors inside next generation CMC-based gas turbine engines will be achievable.

Thermoelectrics based on p-type and n-type films in the Cu-In-O system are currently being fabricated as the continuation of the research presented in chapter 3 of this thesis. Targets have been fabricated using powder processing techniques of the best performing p-type (22 at% In) and n-type (57 at% In) materials from the Cu-In-O system combinatorial library. It is anticipated that the combination of the p-type and n-type Cu-In-O materials will enable the fabrication of a p-n junction for thermoelectric applications comprised of materials from the same system. Additionally, another compound in the Cu-In-O system (22 at% In) was found to exhibit a totally amorphous structure after the film was annealed in nitrogen at 400°C for 5h followed by annealing at 1000°C for 2h in air. Essentially, at this ratio of CuO to In_2O_3, the material maintains its amorphous structure to high temperature, even in the presence of oxygen.

List of References

[1]Ceramic thin film thermocouples for SiC-based ceramic matrix composites, J. D. Wrbanek, G. C. Fralick, and D. Zhu, Thin Solid Films, 2012

BIBLIOGRAPHY

Abdelaziz, Y. A., Megahed, F. M., and Halawa, M. M., "Stability and calibration of platinum-palladium thermocouples following heat treatment," *Measurement*, 2004, pp. 413.

Ahmed, M. G. and Ali, K., "Investigating Pt-Pd Thermocouples in the Temperature Range from 800°C to 1500°C at the National Institute of Standards NIS-Egypt," *Journal of Metrology Society of India*, 2008, pp. 225.

Amani, M., Tougas, I. M., Gregory, O. J., and Fralick, G. C., "Thermoelectric Properties of $Zn_xIn_yO_{x+1.5y}$ Films," *Journal of Electronic Materials*, 2013, pp. 114.

Aniolek, G. E. and Gregory, O. J., "Thin film thermocouples for advanced ceramic gas turbine engines," *Surface and Coatings Technology*, 1994, pp. 70.

Aperathitis, E., Bender, M., Cimalla, V., Ecke, G., and Modreanu, M., "Properties of rf-sputtered indium-tin-oxynitride thin films," *Journal of Applied Physics*, 2003.

Aperathitis, E., Modreanu, M., Bender, M., Cimalla, V., Ecke, G., Androulidaki, M., and Pelekanos, N., "Optical characterization of indium-tin-oxynitride fabricated by RF-sputtering," *Thin Solid Films*, 2004, pp. 101.

Bentley, R. E., "Handbook of Temperature Measurement Vol. 3: Theory and Practice of Thermoelectric Thermometry", *Springer*, 1998.

Bérardan, D., Guilmeau, E., Maignan, M., and Raveau, B., "Enhancement of the thermoelectric performances of In_2O_3 by the coupled substitution of M^{2+}/Sn^{4+} for In^{3+}," *Journal of Applied Physics*, 2008, pp. 064918.

Beszeda, I., Gontier-Moya, E. G., and Beke, D. L., "Investigation of mass transfer surface self-diffusion on palladium," *Surface Science*, 2003, pp. 229.

Bharadwaj, S. R., Kerkar, A. S., Tripathi, S. N., and Dharwadkar, S. R., "The palladium-platinum phase diagram," *Journal of the Less Common Metals*, 1991, pp. 167.

Bosacka, M., Filipek, E., Šulcova, P., Dohnalová, Ž., and Paczesna, A., "Phase equilibria in the solid state and colour properties of the CuO-In_2O_3 system," *Journal of Thermal Analysis and Calorimetry*, 2012, pp. 605.

Burns, G. W., Ripple, D. C., and Battuello, M., "Platinum versus palladium thermocouples – an emf-temperature reference function for the range 0C to 1500C," *Metrologia*, 1998, pp. 761.

Chadwick, A. V., Blacklocks, A. N., Rougier, A., and Yaicle, C., "A Structural Study of Delafossite-type $CuInO_2$ Thin Films," *Journal of Physics: Conference Series,* 2010, pp. 012045.

Chaston, J. C., "The Oxidation of the Platinum Metals – A Descriptive Survey of the Reactions Involved," *Platinum Metals Review,* 1975, pp. 135.

Chen, X., Gregory, O. J., and Amani, M., "Thin-Film Thermocouples Based on the System In_2O_3-SnO_2," *Journal of the American Ceramic Society,* 2011, pp. 854.

Choi, H. And Li, X., "Fabrication and application of micro thin film thermocouples for transient temperature measurement in nanosecond pulsed laser micromachining of nickel," *Sensors and Actuators A,* 2007, pp. 118.

Ellmer, K. and Mientus, R., "Carrier transport in polycrystalline ITO and ZnO:Al II: The influence of grain barriers and boundaries," *Thin Solid Films,* 2008, pp. 5829.

Garino, T. J. and Bowen, H. K., "Kinetics of Constrained-Film Sintering," *Journal of the American Ceramic Society,* 1990, pp. 251.

Gegner, J., Hörz, G., and Kirchheim, R., "Diffusivity and solubility of oxygen in solid palladium," *Journal of Materials Science,* 2009, pp. 2198.

Granqvist, C. G., "Transparent conductors as solar energy materials: A panoramic review," *Solar Energy Materials and Solar Cells*, 2007, pp. 1529.
Gregory, O. J. and Amani, M., "Thermoelectric Properties of $Zn_xIn_yO_{x+1.5y}$ Films," *Journal of the Electrochemical Society*, 2011, pp. J15.

Gregory, O. J., Amani, M., Tougas, I. M., and Drehman, A. J., "Stability and Microstructure of Indium Tin Oxynitride Thin Films," *Journal of the American Ceramic Society,* 2012, pp. 705.

Gregory, O. J., Lee, S. B., Flagan, R. C., "Reaction Sintering of Submicrometer Silicon Powder," *Journal of the American Ceramic Society,* 1987, pp. C52.

Gregory, O. J., Luo, Q., and Crisman, E. E., "High Temperature Stability of Indium Tin Oxide Thin Films," *Thin Solid Films,* 2002, pp. 286.

Gregory, O. J. and You, T., "Piezoresistive Properties of ITO Strain Sensors Prepared with Controlled Nanoporosity," *Journal of the Electrochemical Society,* 2004, pp. H198.

Harvey, S. P., Mason, T.O., Gassenbauer, Y., Schafranek, R., and Klein, A., "Surface versus bulk electronic/defect structures of transparent conducting oxides: I. Indium oxide and ITO," *Journal of Physics D: Applied Physics,* 2006, pp. 3959.

Hill, K. D., "An investigation of palladium oxidation in the platinum-palladium thermocouple system," *Metrologia*, 2002, pp. 51.

Hopper, E. M., Zhu, Q., Song, J-H., Peng, H., Freeman, A. J., and Mason, T. O., "Electronic and thermoelectric analysis of phases in the $In_2O_3(ZnO)_k$ system," *Journal of Applied Physics*, 2011, pp. 013713.

Jehn, H., "High Temperature Behavior of Platinum Group Metals in Oxidizing Atmospheres, *Journal of the Less Common Metals*, 1984, pp. 321.

Jonker, G., "The application of combined conductivity and Seebeck-effect plots for the analysis of semiconducting properties," *Philips Journal of Research*, 1968, pp. 131.

Kaga, H., Asahi, R., and Tani, T., "Thermoelectric Properties of Doped $(ZnO)_mIn_2O_3$," *Japanese Journal of Applied Physics*, 2004, pp. 3540.

Kawazoe, H., Yasukawa, M., Hyodo, H., Kurita, M., Yanagi, H., and Hosono, H., "P-type electrical conduction in transparent thin films of $CuAlO_2$," *Nature*, 1997, pp. 939.

Kim, K. C., Lee, J. H., Kim, J. J., Ikegami, T., "Rapid rate sintering of nanocrystalline indium tin oxide ceramics: particle size effect," *Materials Letters*, 2002, pp. 114.

Kreider, K. G., "Sputtered high temperature thin film thermocouples," *Journal of Vacuum Science Technology*, 1993, pp. 1401.

Kreider, K. G. and DiMeo, F., "Platinum-palladium thin-film thermocouples for temperature measurements on silicon wafers," *Sensors and Actuators, A*, 1998, pp. 46.

Kreider, K. G. and Gillen, G., "High temperature materials for thin-film thermocouples on silicon wafers," *Thin Solid Films*, 2000, pp. 32.

Lee, J-C., Heo, Y-W., Lee, J-H., and Kim, J-J., "Growth of $CuInO_2$ thin film using highly dense Cu_2O-In_2O_3 composite targets," *Thin Solid Films*, 2009, pp. 1234.

Lei, J. F. and Will, H. A., "Thin-Film Thermocouples and Strain-Gauge Technologies for Engine Applications," *Sensors and Actuators A*, 1998, pp. 187.

Liu, L., Bai, K., Gong, H., and Wu, P., "First-Principles Study of Bipolar Dopability in the $CuInO_2$ Transparent Semiconductor," *Chemistry of Materials*, 2005, pp. 5529.

Martin, L. C. and Holanda, R., "Applications of Thin Film Thermocouples for Surface Temperature Measurement," *NASA TM-106714*, 1994.

Medvedovski, E., Szepesi, C. J., Yankov, O., Lippens, P., "Indium tin oxide nanosized transparent conductive thin films obtained by sputtering from large size planar and rotary targets," *Ceramic Transactions*, 2010, pp. 125.

Moiseeva, N. P., "The prospect for developing standard thermocouples of pure metals," *Measurement Science and Technology*, 2004, pp. 915.

Nomura, K., Ohta, H., Takagi, A., Kamiya, T., Hirano, M., and Hosono, H., Amorphous Oxide Semiconductors for High-Performance Flexible Thin-Film Transistors," *Nature*, 2004, pp. 4308.

Omega Engineering, "Revised Thermocouple Reference Tables: Type S," Stamford, CT, [http://www.omega.com/temperature/Z/pdf/z208-209.pdf].

Shimode, M., Sasaki, M., Mukaida, K., "Synthesis of the Delafossite-Type $CuInO_2$," *Journal of Solid State Chemistry*, 2000, pp. 16.

Varela, J. A., Whittemore, O. J., Longo, E., "Pore size evolution during sintering of ceramic oxides," *Ceramics International*, 1990, pp. 177.

Wang, D. and Schaaf, P., "Two-dimensional nanoparticle arrays formed by dewetting of thin gold films deposited on pre-patterned substrates," *Journal of Materials Science: Materials in Electronics*, 2011, pp. 1067.

Wrbanek, J. D., Fralick, G. C., and Zhu, D., "Ceramic thin film thermocouples for SiC-based ceramic matrix composites," *Thin Solid Films*, 2012, pp. 5801.

Yanagi, H., Hase, T., Ibuki, S., Ueda, K., and Hosono, H., "Bipolarity in electrical conduction of transparent oxide semiconductor $CuInO_2$ with delafossite structure," *Applied Physics Letters*, 2001, pp. 1583.

Yin, M., Wu, C-K., Lou, Y., Burda, C., Koberstein, J. T., Zhu, Y., and O'Brien, S., "Copper Oxide Nanocrystals," *Journal of the American Chemical Society*, 2005, pp. 9506.